GENERAL CIRCULATION EXPERIMENTS WITH A TWO-LEVEL QUASI-GEOSTROPHIC MODEL INCLUDING NONLINEAR INTERACTION BETWEEN TWO WAVES AND THE MEAN FLOW

Glenn Curtis Trumbower

NAVAL POSTGRADUATE SCHOOL

Monterey, California

THESIS

General Circulation Experiments with a Two-Level Quasi-Geostrophic Model Including Nonlinear Interaction between Two Waves and the Mean Flow

by

Glenn Curtis Trumbower

Thesis Advisor: R. T. Williams

March 1972

Approved for public release; distribution unlimited.

General Circulation Experiments with a Two-Level Quasi-Geostrophic Model Including Nonlinear Interaction between Two Waves and the Mean Flow

by

Glenn Curtis Trumbower
Lieutenant, United States Navy
B.S., Florida State University, 1967

Submitted in partial fulfillment of the
requirements for the degree of

MASTER OF SCIENCE IN METEOROLOGY

from the

NAVAL POSTGRADUATE SCHOOL
March 1972

ABSTRACT

Long term numerical integrations were performed with a two-level model utilizing the quasi-geostrophic equation set. Friction was incorporated through the vertical derivative of the eddy stress and heating was applied as a linear function of latitude. The long-term interactions between one or two waves in the zonal direction and the mean flow were examined.

The stability of the initial mean flow was investigated with linearized equations and the most unstable wave numbers were determined. The nonlinear equations were integrated using the most unstable wave in the initial conditions. 300 day forecasts were made with various values of the heating, β, wall separation, and wave number. A second wave number was introduced into the experiments in order to determine the most likely wave number for the fully evolved mean flow. Constant amplitude, baroclinic, propagating disturbances were obtained in every case where the wall separation was 4,000 km. The experiments with the wall separation of 8,000 km produced non-steady waves with fluctuating baroclinic and barotropic interactions.

TABLE OF CONTENTS

TABLE OF SYMBOLS AND ABBREVIATIONS

β_o	Derivative of coriolis parameter at mid-latitude
γ	Eddy viscosity
C_p	Specific heat at constant pressure
C_D	Drag coefficient
f_o	Coriolis parameter at mid-latitude
g	Gravity
ω	dp/dt
R	Gas constant
ρ	Density
$\bar{T}$	Average temperature from standard atmosphere
σ	$(R^2\bar{T}/p^2 g)\ (\partial\bar{T}/\partial z + g/C_p)$
ζ	$\frac{1}{f_o}\nabla^2\phi$
z	Height
$\varkappa$	R/C_p
S	Heating added per unit mass
W	Distance between the walls
τ	Eddy stress
ϕ	gz
q	Potential vorticity

ACKNOWLEDGEMENTS

The author wishes to express his deep appreciation and thanks to Dr. R. Terry Williams whose interest, counsel, and recommendations were truly exceptional.

I would further like to thank Dr. George J. Haltiner for his assistance and suggestions which contributed to this study. A thank you is also offered to Frank H. Taylor, portions of whose April 1970 thesis results and model were used in this paper.

I. INTRODUCTION

In a classic experiment, Phillips (1956) performed a long-period numerical forecast with a two-level quasi-geostrophic model in a zonally periodic channel on a Beta plane. Friction and heating were included in his model with the latter as a linear function of latitude. Although Phillips' experiment did not reach statistical equilibrium, he demonstrated that the principal features of the general circulation of the atmosphere could be reproduced with a simple numerical model. More refined studies involving the primitive equations have been carried out by Smagorinsky (1963), Mintz (1965), Manabe and Smagorinsky (1967), Manabe (1969), and Kasahara and Washington (1967) and (1971). These studies which more accurately model the actual atmosphere are sufficiently complicated so that it is difficult to understand the basic interactions between the mean flow and the disturbances.

For this reason, we wish to re-examine Phillips' original simple model. In this study, Phillips' model is further simplified to represent the x-variation of the disturbance with one or two Fourier components. This restriction is partially justified by the fact that one predominate wave number was observed. Similarily, in dish-pan experiments with inner cores, single wave numbers were observed in many instances; see Fultz (1959) and Hide (1953). Herring (1963) and (1964) has used the technique of examining the interaction between a disturbance of sinusoidal variation and a mean field in his study of convection between two rigid plates. His estimates of the heat fluxes between the plates were within 20% of the value obtained from laboratory experiments.

This suggests that a simplified dynamic model of the atmosphere which involves the interaction between a simplified disturbance and a mean flow can give reasonable approximations of the northward fluxes of heat and momentum.

Therefore, in this study, the complexities have been kept to a minimum to simplify interpretation of the interactions. The two-level model utilizes the quasi-geostrophic equation set. Fluid motion in the model is restricted to the mean flow and one or two wave numbers. The mean flow and Fourier amplitudes of the two disturbances are allowed to vary in time and y-space; hence an adequate description of barotropic as well as baroclinic interactions are possible.

However, such a drastically simplified model must omit many details of the real atmosphere. In the case of this model, a number of physical properties of the earth's atmosphere are missing. Two waves in juxtaposition will not interact directly, but can only influence each other through the modification of the mean flow. No oceans, moisture, mountains, or east-west heating gradient are allowed in the model. Consequently, this model appears to be one of the simplest models which can describe some of the principal mechanisms of the general circulation.

II. THE MODEL AND FORECAST EQUATIONS

The model used in these experiments utilizes the simple two-level, quasi-geostrophic equation set. The atmosphere is divided into four layers of thickness $\Delta p/2$, numbered 0 to 4 in Figure 1.

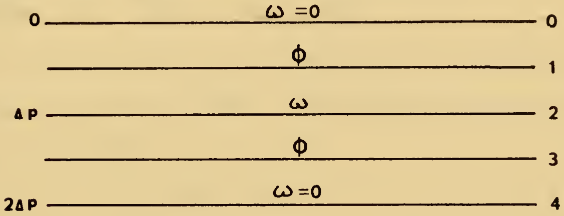

Fig. 1. Two-level model.

The earth's surface is assumed to be a smooth, flat, land surface with no oceans. Therefore, the vertical motion at the top and bottom of the atmosphere is taken to be zero.

Internal friction is represented by the vertical derivative of the eddy stress τ.

The quasi-geostrophic vorticity and thermodynamic equations are

$$\frac{\partial \zeta}{\partial t} + \mathbb{V} \cdot \nabla \zeta + \beta_o v - f_o \frac{\partial \omega}{\partial p} = - \mathbb{k} \cdot \nabla \times g \frac{\partial \tau}{\partial p} \qquad (2.1)$$

$$\frac{\partial}{\partial t} \frac{\partial \phi}{\partial p} + \mathbb{V} \cdot \nabla \frac{\partial \phi}{\partial p} + \omega \sigma = - \frac{\kappa S}{p} \qquad (2.2)$$

where $\kappa = R/C_p$, S = net heating from radiation, and σ, the static stability, is

$$\sigma \equiv \frac{R^2 \bar{T}}{p^2 g} [\gamma_d - \gamma] = \frac{R^2 \bar{T}}{p^2 g} [\frac{g}{C_p} + \frac{dT}{dZ}] = 2.3 m^2 s^{-2} cb^{-2} \qquad (2.3)$$

T is taken from a standard atmosphere.

Apply Equation (2.1) at levels 1 and 3, which yields

$$\frac{\partial \zeta_1}{\partial t} + \mathbb{V}_1 \cdot \nabla \zeta_1 + \beta_o v_1 - f_o \frac{\omega_2}{\Delta p} = \frac{-g}{\Delta p} \mathbf{k} \cdot \nabla \times (\tau_2 - \tau_o) \tag{2.4}$$

$$\frac{\partial \zeta_3}{\partial t} + \mathbb{V}_3 \cdot \nabla \zeta_3 + \beta_o v_3 + f_o \frac{\omega_2}{\Delta p} = \frac{-g}{\Delta p} \mathbf{k} \cdot \nabla \times (\tau_4 - \tau_2) \tag{2.5}$$

If we apply Equation (2.2) at level 2, we obtain

$$\frac{\partial}{\partial t}\left(\frac{\partial \phi}{\partial p}\right)_2 + \mathbb{V}_2 \cdot \nabla \left(\frac{\partial \phi}{\partial p}\right)_2 + \omega_2 \sigma = \frac{-\kappa S_2}{\Delta p} \tag{2.6}$$

The heating function, S_2, is restricted to a linear function in y as utilized by Phillips (1956). The model has heating in the south and cooling in the north.

$$S_2 \equiv h\left(\frac{w}{2} - y\right)/w \tag{2.7}$$

where w is the north-south wall separation distance.

The amount of net heating is proportional to h which varies from 0.001 to 0.016 kilojoules ton^{-1} sec^{-1}.

The eddy stress τ_o at the top of the atmosphere is taken to be zero. The eddy stress term τ_2 at level 2, takes the form

$$\tau_2 \equiv - \rho^2 g \gamma \frac{\partial \mathbb{V}}{\partial p} \tag{2.8}$$

where γ is the eddy viscosity. If we follow Smagorinsky (1963), the finite difference form becomes

$$\tau_2 = -(\rho\gamma)_2 \, (g\rho_2/\Delta p) \, (\mathbb{V}_3 - \mathbb{V}_1) \tag{2.9}$$

where $(\rho_2 g/\Delta p) = 1/7.9 \text{ km}^{-1}$ is the inverse depth of the 750-250mb layer and $(\rho\gamma)_2 = \begin{Bmatrix} 50 \\ 225 \\ 500 \end{Bmatrix} \times 10^{-4}$ ton m^{-1} s^{-1} is an exchange coefficient. The smallest estimates of $(\rho\gamma)_2$ was proposed by Rossby and Montgomery (1935) for stable conditions, while the largest was utilized by Riehl (1951). The intermediate value, 225, was proposed by Palmen (1955).

Thus, the stress term at level 2 becomes

$$\tau_2 = - C_2 (\mathbb{V}_3 - \mathbb{V}_1) \qquad (2.10)$$

where $C_2 = \begin{Bmatrix} 50 \\ 225 \\ 500 \end{Bmatrix} \times 10^{-6}/79 \text{ ton s}^{-1}$ (2.11)

The majority of the experiments were conducted using Palmen's exchange coefficient of 225.

The eddy stress term τ_4 at the surface, level 4, as formulated by Phillips (1956) is assumed to be in the direction of the surface wind and proportional to the square of the wind speed.

$$\tau_4 \equiv \frac{\rho}{2} C_D |\mathbb{V}_4| \mathbb{V}_4 \qquad (2.12)$$

where C_D is the drag coefficient = 0.015.

The surface geostrophic vorticity is approximated by the 750mb vorticity

$$\zeta_4 \doteq \zeta_3 = \frac{1}{f_o} \nabla^2 \phi_3$$

thus $\mathbb{V}_4 \doteq \mathbb{V}_3$.

So, by defining $C_4 = \frac{\rho}{2} C_D |\mathbb{V}_4|$ (2.13)

$$\tau_4 = C_4 \mathbb{V}_3 \qquad (2.14)$$

The average value of the 750mb wind speed was taken to be 5 m s^{-1}.

Thus, our assumptions make τ_4 a linear function of wind speed with

$$C_4 = 3.69 \times 10^{-5} \text{ ton s}^{-1} \qquad (2.15)$$

Therefore, as boundary conditions at the top, internal, and bottom layers of the atmosphere

$$\omega_o = \omega_4 = 0$$

$$\tau_o = 0$$

$$\tau_2 = - C_2 (\mathbb{V}_3 - \mathbb{V}_1)$$

$$\tau_4 = C_4 \, \mathbb{V}_3$$

For convenience, the following quantities are defined

$$\phi_M \equiv \frac{\phi_1 + \phi_3}{2} \qquad (2.16)$$

$$\phi_T \equiv \frac{\phi_1 + \phi_3}{2} \qquad (2.17)$$

implies

$$\phi_1 = \phi_M + \phi_T \qquad \phi_3 = \phi_M - \phi_T$$

$$\zeta_M = \frac{\zeta_1 + \zeta_3}{2} \qquad \zeta_T = \frac{\zeta_1 - \zeta_3}{2}$$

$$\zeta_1 = \zeta_M + \zeta_T \qquad \zeta_3 = \zeta_M - \zeta_T$$

the mean quantities may be interpreted as applying at level 2.

Integrate the hydrostatic equation $\frac{\partial \phi}{\partial p} = - \alpha$ from level 1 to 3, which yields

$$\phi_T = \frac{R\overline{T}}{2} \ln (P_3/P_1) \qquad (2.18)$$

Equation (2.18) shows that ϕ_T is proportional to the mean temperature of the layer.

If (2.16) and (2.17) are introduced into the thermodynamic equation (2.6), we obtain

$$\frac{\partial}{\partial t} \phi_T + \mathbb{V}_M \cdot \nabla \phi_T - \frac{\omega_2 \sigma \Delta p}{2} = \frac{\kappa S_2}{2} \qquad (2.19)$$

The mean vorticity equation is obtained by adding Equation (2.4) and (2.5) and dividing by two.

$$\frac{\partial}{\partial t} \zeta_M + \mathbb{V}_M \cdot \nabla \zeta_M + \mathbb{V}_T \cdot \nabla \zeta_T + \beta_o v_M = \frac{-g}{2\Delta p} \mathbb{k} \cdot \nabla \times \tau_4 \qquad (2.20)$$

The thermal vorticity equation is obtained by subtracting Equation (2.4) from (2.5) and dividing by two.

$$\frac{\partial}{\partial t}\zeta_T + \mathbf{V}_M \cdot \nabla\zeta_T + \mathbf{V}_T \cdot \nabla\zeta_M + \beta_o v_T - f_o \frac{\omega_2}{\Delta p} = - \frac{g}{\Delta p}\mathbf{k} \cdot \nabla \times \tau_2 + \frac{g}{2\Delta p}\mathbf{k} \cdot \nabla \times \tau_4 \tag{2.21}$$

Solve (2.19) for ω_2 and apply this solution to the thermal vorticity equation (2.21).

Substitute the following geostrophic relations

$$\mathbf{V} = \frac{1}{f_o}\mathbf{k} \times \nabla \phi , \qquad \zeta = \frac{1}{f_o} \nabla^2 \phi$$

into Equation (2.20) and multiply by f_o, which becomes the Mean Vorticity Equation:

$$\frac{\partial}{\partial t} \nabla^2\phi_M + \frac{1}{f_o} (\mathbf{k} \times \nabla\phi_M) \cdot \nabla(\nabla^2\phi_M) + \frac{1}{f_o} (\mathbf{k} \times \nabla\phi_T)\cdot\nabla(\nabla^2 \phi_T) + \beta_o \frac{\partial\phi_M}{\partial x} - K_4 (\nabla^2\phi_T - \nabla^2\phi_M) = 0 \tag{2.22}$$

Introduce the geostrophic relations for $\mathbf{V}$ and ζ into (2.21) and multiply by f_o, which gives the Thermal Vorticity Equation:

$$\frac{\partial}{\partial t}(\nabla^2 - \mu^2) \phi_T + \frac{1}{f_o} (\mathbf{k} \times \nabla\phi_M) \cdot \nabla(\nabla^2 - \mu^2) \phi_T + \frac{1}{f_o} (\mathbf{k} \times \nabla\phi_T) \cdot \nabla(\nabla^2\phi_M) - \beta_o \frac{\partial\phi_T}{\partial x} + K_4(\nabla^2\phi_T - \nabla^2\phi_M) + \mu^2 \frac{\varkappa S_2}{2} = - K_2 \nabla^2\phi_T \tag{2.23}$$

where

$$\mu^2 \equiv \frac{2f_o^{\,2}}{(\Delta p)^2\sigma} = 3.48 \times 10^{-12} \ m^{-2} \tag{2.24}$$

$$K_2 \equiv \frac{C_4 g}{2\Delta p} = 1.12 \times 10^{-6} \ s^{-1} \tag{2.25}$$

$$K_4 \equiv \frac{2C_2 g}{\Delta p} = 3.59 \times 10^{-6} \ s^{-1} \tag{2.26}$$

It can be seen that the frictional coefficient at the surface is roughly three times as large as the internal coefficient.

The mean and thermal vorticity equations (2.22) and (2.23) are the prediction equations in the two unknowns ϕ_T and ϕ_M. At this point, the geopotential height fields are restricted as follows:

$$\phi_M \equiv E(y,t) + A(y,t) \cos kx + B(y,t) \sin kx$$
$$+ G(y,t) \cos mx + H(y,t) \sin mx \tag{2.27}$$

$$\phi_T \equiv F(y,t) + C(y,t) \cos kx + D(y,t) \sin kx$$
$$+ P(y,t) \cos mx + Q(y,t) \sin mx \tag{2.28}$$

where E(y,t) and F(y,t) are the amplitudes of the zonal mean flow; A(y,t), B(y,t), C(y,t), and D(y,t) are the Fourier amplitudes of the disturbance of wave number k, and G(y,t), H(y,t), P(y,t), and Q(y,t) are the Fourier amplitudes of the disturbance of wave number m. Both waves are in the x-direction only.

Since E and F are functions of y, barotropic instability is possible in this system as well as baroclinic instability. If the definitions of ϕ_T and ϕ_M are substituted into $\mathbb{V} = \frac{1}{f_o} \mathbb{k} \times \nabla\phi$, we obtain:

$$u_M = -\frac{1}{f_o}\frac{\partial\phi_M}{\partial y} \qquad v_M = \frac{1}{f_o}\frac{\partial\phi_M}{\partial x} \tag{2.29}$$

$$\bar{u}_M = -\frac{1}{f_o}\frac{\partial E}{\partial y} \qquad \bar{v}_M = \frac{1}{f_o}\frac{\partial E}{\partial x} = 0 \tag{2.30}$$

$$u_T = -\frac{1}{f_o}\frac{\partial\phi_T}{\partial y} \qquad v_T = \frac{1}{f_o}\frac{\partial\phi_T}{\partial x} \tag{2.31}$$

$$\bar{u}_T = -\frac{1}{f_o}\frac{\partial F}{\partial y} \qquad \bar{v}_T = \frac{1}{f_o}\frac{\partial F}{\partial x} = 0 \tag{2.32}$$

where the bar $(\bar{\ })$ indicates the x-average.

At the north and south boundaries, the following conditions are imposed initially and for all time:

$$u_M = u_T = \bar{u}_M = \bar{u}_T = 0 \qquad \text{at } y = 0,\ y = W$$

$$\frac{\partial u_M}{\partial t} = \frac{\partial u_T}{\partial t} = \frac{\partial \bar{u}_M}{\partial t} = \frac{\partial \bar{u}_T}{\partial t} = 0 \qquad \text{at } y = 0,\ y = W$$

where W is the northern boundary.

Substitute (2.27) and (2.28) into the mean vorticity (2.22) and thermal vorticity (2.23) equations. Now if we separate the various terms, and neglect all terms of wave number 2k and 2m and combinations of m and k, we obtain ten equations in ten unknowns.

When we equate the coefficients of the cos kx terms of (2.22), we obtain:

$$\frac{\partial}{\partial t}\left(\frac{\partial^2}{\partial y^2}-k^2\right)A = \frac{k}{f_o}\left[\frac{\partial^2 B}{\partial y^2}\frac{\partial E}{\partial y} + \frac{\partial^2 D}{\partial y^2}\frac{\partial F}{\partial y} - B\frac{\partial^3 E}{\partial y^3} - D\frac{\partial^3 F}{\partial y^3} - k^2\left(B\frac{\partial E}{\partial y} + D\frac{\partial F}{\partial y}\right)\right]$$
$$- \beta_o Bk - K_4\left(\frac{\partial^2}{\partial y^2} - k^2\right)(A - C) \tag{2.33}$$

The sin kx terms of (2.22) give:

$$\frac{\partial}{\partial t}\left(\frac{\partial^2}{\partial y^2}-k^2\right)B = \frac{k}{f_o}\left[-\frac{\partial^2 A}{\partial y^2}\frac{\partial E}{\partial y} - \frac{\partial^2 C}{\partial y^2}\frac{\partial F}{\partial y} + A\frac{\partial^3 E}{\partial y^3} + C\frac{\partial^3 F}{\partial y^3} + k^2\left(A\frac{\partial E}{\partial y} + C\frac{\partial F}{\partial y}\right)\right]$$
$$+ \beta_o Ak - K_4\left(\frac{\partial^2}{\partial y^2} - k^2\right)(B - D) \tag{2.34}$$

The cos kx terms of (2.23) give:

$$\frac{\partial}{\partial t}\left(\frac{\partial^2}{\partial y^2}-k^2-\mu^2\right)C = \frac{k}{f_o}\left[\frac{\partial E}{\partial y}\frac{\partial^2 D}{\partial y^2} + \frac{\partial F}{\partial y}\frac{\partial^2 B}{\partial y^2} - \frac{\partial E}{\partial y}D(k^2+\mu^2) - \frac{\partial F}{\partial y}B(k^2-\mu^2)\right.$$
$$\left. - \frac{\partial^3 E}{\partial y^3}D - \frac{\partial^3 F}{\partial y^3}B\right] - \beta_o Dk + K_4\left(\frac{\partial^2}{\partial y^2}-k^2\right)(A-C)$$
$$+ K_2\left(Ck^2 - \frac{\partial^2 C}{\partial y^2}\right) \tag{2.35}$$

The sin kx terms of (2.23) give:

$$\frac{\partial}{\partial t}\left(\frac{\partial^2}{\partial y^2}-k^2-\mu^2\right)D = \frac{k}{f_o}\left[-\frac{\partial E}{\partial y}\frac{\partial^2 C}{\partial y^2} - \frac{\partial F}{\partial y}\frac{\partial^2 A}{\partial y^2} + \frac{\partial E}{\partial y}C(k^2+\mu^2) + \frac{\partial F}{\partial y}A(k^2-\mu^2)\right.$$

$$+ \frac{\partial^3 E}{\partial y^3} C + \frac{\partial^3 F}{\partial y^3} A] + \beta_o Ck + K_4\left(\frac{\partial^2}{\partial y^2} - k^2\right)(B-D) + K_2\left(Dk^2 - \frac{\partial^2 D}{\partial y^2}\right) \tag{2.36}$$

The terms independent of x in (2.22) give:

$$\begin{aligned} \frac{\partial}{\partial t} \frac{\partial^2}{\partial y^2} E = {} & \frac{k}{2f_o} \frac{\partial}{\partial y}\left[A \frac{\partial^2 B}{\partial y^2} - B \frac{\partial^2 A}{\partial y^2} + C \frac{\partial^2 D}{\partial y^2} - D \frac{\partial^2 C}{\partial y^2}\right] \\ & + \frac{m}{2f_o} \frac{\partial}{\partial y}\left[G \frac{\partial^2 H}{\partial y^2} - H \frac{\partial^2 G}{\partial y^2} + P \frac{\partial^2 Q}{\partial y^2} - Q \frac{\partial^2 P}{\partial y^2}\right] \\ & - K_4 \frac{\partial}{\partial y}\left(\frac{\partial E}{\partial y} - \frac{\partial F}{\partial y}\right) \end{aligned} \tag{2.37}$$

The cos mx terms of (2.22) give:

$$\begin{aligned} \frac{\partial}{\partial t}\left(\frac{\partial^2}{\partial y^2} - m^2\right) G = {} & \frac{m}{f_o}\left[\frac{\partial^2 H}{\partial y^2} \frac{\partial E}{\partial y} + \frac{\partial^2 Q}{\partial y^2} \frac{\partial F}{\partial y} - H \frac{\partial^3 E}{\partial y^3} - Q \frac{\partial^3 F}{\partial y^3} - m^2\left(H \frac{\partial E}{\partial y} + Q \frac{\partial F}{\partial y}\right)\right] \\ & - \beta_o Hm - K_4\left(\frac{\partial^2}{\partial y^2} - m^2\right)(G - P) \end{aligned} \tag{2.38}$$

The sin mx terms of (2.22) give:

$$\begin{aligned} \frac{\partial}{\partial t}\left(\frac{\partial^2}{\partial y^2} - m^2\right) H = {} & \frac{m}{f_o}\left[- \frac{\partial^2 G}{\partial y^2} \frac{\partial E}{\partial y} - \frac{\partial^2 P}{\partial y^2} \frac{\partial F}{\partial y} + G \frac{\partial^3 E}{\partial y^3} + P \frac{\partial^3 F}{\partial y^3} + m^2\left(G \frac{\partial E}{\partial y} + P \frac{\partial F}{\partial y}\right)\right] \\ & + \beta_o Gm - K_4\left(\frac{\partial^2}{\partial y^2} - m^2\right)(H - Q) \end{aligned} \tag{2.39}$$

The cos mx terms of (2.23) give:

$$\begin{aligned} \frac{\partial}{\partial t}\left(\frac{\partial^2}{\partial y^2} - m^2 - \mu^2\right) P = {} & \frac{m}{f_o}\left[\frac{\partial E}{\partial y} \frac{\partial^2 Q}{\partial y^2} + \frac{\partial F}{\partial y} \frac{\partial^2 H}{\partial y^2} - \frac{\partial E}{\partial y} Q(m^2 + \mu^2) - \frac{\partial F}{\partial y} H(m^2 - \mu^2)\right. \\ & \left. - \frac{\partial^3 E}{\partial y^3} Q - \frac{\partial^3 F}{\partial y^3} H\right] - \beta_o Qm + K_4\left(\frac{\partial^2}{\partial y^2} - m^2\right)(G-P) + K_2\left(Pm^2 - \frac{\partial^2 P}{\partial y^2}\right) \end{aligned} \tag{2.40}$$

The sin mx terms of (2.23) give:

$$\begin{aligned} \frac{\partial}{\partial t}\left(\frac{\partial^2}{\partial y^2} - m^2 - \mu^2\right) Q = {} & \frac{m}{f_o}\left[- \frac{\partial E}{\partial y} \frac{\partial^2 P}{\partial y^2} - \frac{\partial F}{\partial y} \frac{\partial^2 G}{\partial y^2} + \frac{\partial E}{\partial y} P(m^2 + \mu^2) + \frac{\partial F}{\partial y} G(m^2 - \mu^2)\right. \\ & \left. + \frac{\partial^3 F}{\partial y^3} G + \frac{\partial^3 E}{\partial y^3} P\right] + \beta_o Pm + K_4\left(\frac{\partial^2}{\partial y^2} - m^2\right)(H-Q) + K_2\left(Qm^2 - \frac{\partial^2 Q}{\partial y^2}\right) \end{aligned} \tag{2.41}$$

The coefficients independent of x in (2.23) give:

$$\frac{\partial}{\partial t}\left(\frac{\partial^2}{\partial y^2} - \mu^2\right)F = \frac{k}{2f_o}\,\frac{\partial}{\partial y}\left[A\frac{\partial^2 D}{\partial y^2} - B\frac{\partial^2 C}{\partial y^2} + C\frac{\partial^2 B}{\partial y^2} - D\frac{\partial^2 A}{\partial y^2} + \mu^2(BC - AD)\right]$$
$$+ \frac{m}{2f_o}\,\frac{\partial}{\partial y}\left[G\frac{\partial^2 Q}{\partial y^2} - H\frac{\partial^2 P}{\partial y^2} + P\frac{\partial^2 H}{\partial y^2} - Q\frac{\partial^2 G}{\partial y^2} + \mu^2(HP - GQ)\right]$$
$$+ K_4\,\frac{\partial}{\partial y}\left(\frac{\partial E}{\partial y} - \frac{\partial F}{\partial y}\right) - \mu^2\,\frac{\varkappa S_2}{2} - K_2\,\frac{\partial^2 F}{\partial y^2} \qquad (2.42)$$

Equations (2.33) - (2.42) constitute the prediction formulas.

III. PROCEDURE AND GOALS

The north-south grid distance Δy was set at 200km. A time step, Δt, of 1/2 hour was chosen to allow wind speeds up to 100 m s^{-1} with computational stability.

Centered time differences were used for all quantities except those involving friction. The frictional terms were computed at time $t - \Delta t$. The first time step was a forward step. The Euler-backward time step was introduced every 24 hours to selectively damp high frequency waves. These waves are produced by the separation of solutions at even and odd time steps caused by the leap-frog time scheme.

The finite difference scheme used is illustrated below with the function F,

$$\frac{\partial F}{\partial y} = \frac{1}{2\Delta y}(F_{j+1} - F_{j-1})$$

$$\frac{\partial^2 F}{\partial y^2} = \frac{1}{(\Delta y)^2}(F_{j+1} - 2F_j + F_{j-1})$$

$$\frac{\partial^3 F}{\partial y^3} = \frac{1}{2(\Delta y)^3}[(F_{j+2} - 2F_{j+1} + F_j) - (F_j - 2F_{j-1} + F_{j-2})]$$

where j is the grid index and Δy the distance between grid points (200km).

Equations (2.33) through (2.42) except (2.37) were solved by a Gauss pivotal elimination matrix method described by Richtmyer (1957). Equation (2.37) was solved by a direct marching process).

The model was run as a Beta-plane experiment with periodic east-west motion between north-south walls of separation W, 4,000 or 8,000 km.

The 8,000 km experiments were likened to the atmosphere. It was hoped the mean temperature gradient from the north to south boundary at level 2 would be comparable to that of the atmosphere at 500 mb. The source of available potential energy, $(\overline{S}\cdot\overline{P})$, should yield a value not much less than 60% of the atmosphere's total zonal generation of 56×10^{-4} kj m^{-2} s^{-1} formalized by Dutton and Johnson (1967). It should be noted that this model contains no east-west heating gradient; therefore, conversion of heat into available potential energy (APE) will be less than observed.

Lastly, the winds at 250 mb should exhibit a jet structure and the 750 mb winds portray the belts of zonal easterlies and westerlies.

IV. VERTICAL MOTION EQUATIONS

Vertical motion at 500 mb is calculated through the thermodynamic equation (2.19).

$$\begin{aligned}\omega_2 = \frac{2}{\Delta p\sigma}\Bigg\{ & \cos kx\Big[\frac{\partial C}{\partial t} - \frac{k}{f_o}\Big(D\frac{\partial E}{\partial y} - B\frac{\partial F}{\partial y}\Big)\Big] + \sin kx\Big[\frac{\partial D}{\partial t} + \frac{k}{f_o}\Big(C\frac{\partial E}{\partial y} - A\frac{\partial F}{\partial y}\Big)\Big] \\ & + \cos mx\Big[\frac{\partial P}{\partial t} - \frac{m}{f_o}\Big(Q\frac{\partial E}{\partial y} - H\frac{\partial F}{\partial y}\Big)\Big] + \sin mx\Big[\frac{\partial Q}{\partial t} + \frac{m}{f_o}\Big(P\frac{\partial E}{\partial y} - G\frac{\partial F}{\partial y}\Big)\Big] \\ & + \frac{\partial F}{\partial t} - \frac{\varkappa S_2}{2}\Bigg\} + \frac{1}{\Delta p\sigma f_o}\Bigg\{k\Big[-D\frac{\partial A}{\partial y} + B\frac{\partial C}{\partial y} + C\frac{\partial B}{\partial y} - A\frac{\partial D}{\partial y}\Big] \\ & + m\Big[-Q\frac{\partial G}{\partial y} + H\frac{\partial P}{\partial y} + P\frac{\partial H}{\partial y} - G\frac{\partial Q}{\partial y}\Big]\Bigg\} \qquad (4.1)\end{aligned}$$

all terms of wave number 2k or 2m and combinations of m and k have been neglected.

The vertical motion, ω, can be written as

$$\omega = \bar{\omega} + \omega'$$

where the average vertical motion is

$$\bar{\omega} = \frac{2}{\Delta p\sigma}\left\{\frac{\partial F}{\partial t} - \frac{\varkappa S_2}{2} + \frac{1}{2f_o}\left[k\frac{\partial}{\partial y}(BC - AD) + m\frac{\partial}{\partial y}(PH - GQ)\right]\right\} \qquad (4.2)$$

again, the barred quantity means x-averaged.

The disturbance vertical motion, ω', is given by

$$\omega' = \omega'_c\,(\cos kx) + \omega'_s(\sin kx) + \omega'_c(\cos mx) + \omega'_s(\sin mx) \qquad (4.3)$$

where

$$\omega'_c(\cos kx) \equiv \frac{2}{\sigma\Delta p}\left\{\cos kx\left[\frac{\partial C}{\partial t} - \frac{k}{f_o}\left(D\frac{\partial E}{\partial y} - B\frac{\partial F}{\partial y}\right)\right]\right\} \qquad (4.4)$$

$$\omega'_s(\sin kx) \equiv \frac{2}{\sigma\Delta p}\left\{\sin kx\left[\frac{\partial D}{\partial t} + \frac{k}{f_o}\left(C\frac{\partial E}{\partial y} - A\frac{\partial F}{\partial y}\right)\right]\right\} \qquad (4.5)$$

$$\omega'_c(\cos mx) \equiv \frac{2}{\sigma\Delta p}\left\{\cos mx\left[\frac{\partial P}{\partial t} - \frac{m}{f_o}\left(Q\frac{\partial E}{\partial y} - H\frac{\partial F}{\partial y}\right)\right]\right\} \qquad (4.6)$$

$$\omega'_s(\sin mx) \equiv \frac{2}{\sigma\Delta p}\left\{\sin mx\left[\frac{\partial Q}{\partial t} + \frac{m}{f_o}\left(P\frac{\partial E}{\partial y} - G\frac{\partial F}{\partial y}\right)\right]\right\} \qquad (4.7)$$

V. COMPUTATION OF AVERAGE NORTH-SOUTH WIND

The average north-south flow computations coupled with the average vertical motion provides one with a fast method of calculating the circulation in the meridional plane; i.e. Hadley or Ferrel cells.

If we apply the continuity equation at level 1, we obtain

$$\frac{\partial \bar{\omega}_2}{\partial p} = - \nabla \cdot \bar{\mathbb{V}}_1 \qquad (5.1)$$

$$\frac{\partial \bar{v}_1}{\partial y} = - \frac{\partial \bar{\omega}_2}{\partial p} \qquad (5.2)$$

Thus, the finite difference form is

$$(\bar{v}_1)_1 = (\bar{v}_1)_j - \frac{\Delta y}{\Delta p} \left[\frac{(\bar{\omega}_2)_j + (\bar{\omega}_2)_{j+1}}{2}\right] \qquad (5.3)$$

where $(\bar{v}_1)_1 = 0$.

VI. ENERGY AND ENERGY TRANSFORMATION EQUATIONS

The energy equations were obtained from Phillips (1956).

Mean Potential Energy per unit mass,

$$\overline{P} \equiv \frac{\mu^2}{8Wf_o^2}\int(\overline{\phi}_1 - \overline{\phi}_3)^2 dy \tag{6.1}$$

Disturbance Potential Energy per unit mass,

$$P' \equiv \frac{\mu^2}{8Wf_o^2}\int(\phi_1' - \phi_3')^2 dy \tag{6.2}$$

Mean Kinetic Energy per unit mass,

$$\overline{K} \equiv \frac{1}{4W}\int(\overline{u}_1^2 + \overline{u}_3^2)dy \tag{6.3}$$

Disturbance Kinetic Energy per unit mass,

$$K' \equiv \frac{1}{4Wf_o^2}\int[(\nabla\phi_1')^2 + (\nabla\phi_3')^2]\, dy \tag{6.4}$$

If we substitute the ϕ_T and ϕ_M into the above energy equations, we obtain

$$\overline{P} = \frac{\mu^2}{2Nf_o^2}\sum_{j=0}^{N} F_j^2$$

$$P'(k) = \frac{\mu^2}{4Nf_o^2}\sum_{j=0}^{N}(C_j^2 + D_j^2) \qquad P'(m) = \frac{\mu^2}{4Nf_o^2}\sum_{j=0}^{N}(P_j^2 + Q_j^2)$$

$$\overline{K} = \frac{1}{2Nf_o^2}\sum_{j=0}^{N}\left[\left(\frac{\partial E}{\partial y}\right)_j^2 + \left(\frac{\partial F}{\partial y}\right)_j^2\right]$$

$$K'(k) = \frac{1}{4Nf_o^2}\sum_{j=0}^{N}\left[k^2(A_j^2 + B_j^2 + C_j^2 + D_j^2) + \left(\frac{\partial A}{\partial y}\right)_j^2 + \left(\frac{\partial B}{\partial y}\right)_j^2 + \left(\frac{\partial C}{\partial y}\right)_j^2 + \left(\frac{\partial D}{\partial y}\right)_j^2\right]$$

$$K'(m) = \frac{1}{4Nf_o^2} \sum_{j=0}^{N} [m^2(G_j^2 + H_j^2 + P_j^2 + Q_j^2) + (\frac{\partial G}{\partial y})_j^2 + (\frac{\partial H}{\partial y})_j^2$$

$$+ (\frac{\partial P}{\partial y})_j^2 + (\frac{\partial Q}{\partial y})_j^2]$$

where the subscripts k and m stand for wave number, and N is the number of grid increments such that

$$W = N\Delta y$$

Following the procedure of Phillips (1956), the energy flow diagram of Figure 2 should make the physical interpretation of the energy transformation equations clear.

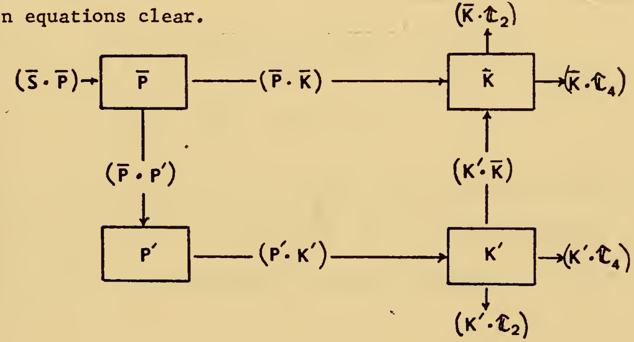

Fig. 2. Energy Flow Diagram

The flow of energy is in the direction of the arrows if the associated transformation (•) is positive.

The energy transformation equations are:

$$(\bar{S}\cdot\bar{P}) = \frac{\mu^2\varkappa}{2Nf_o^2} \sum_{j=0}^{N} (S_j \cdot F_j)$$

$$(\bar{P}\cdot P')(k) = \frac{\mu^2 k}{2Nf_o^3} \sum_{j=0}^{N} [(A\cdot D - B\cdot C)_j \cdot (\frac{\partial F}{\partial y})_j]$$

$$(P'\cdot K')(k) = \frac{-1}{2\Delta p\ N} \sum_{j=0}^{N} [C_j\omega'_{cj}(\cos kx) + D_j\omega'_{sj}(\sin kx)]$$

$$(K'\cdot\bar{K}) = \frac{-k}{2f_o^{\,3}N}\sum_{j=0}^{N}\Big[\Big(\frac{\partial E}{\partial y}\Big)_j\Big(B\frac{\partial^2 A}{\partial y^2} - A\frac{\partial^2 B}{\partial y^2} + D\frac{\partial^2 C}{\partial y^2} - C\frac{\partial^2 D}{\partial y^2}\Big)_j$$

$$+ \Big(\frac{\partial F}{\partial y}\Big)_j\Big(B\frac{\partial^2 C}{\partial y^2} - A\frac{\partial^2 D}{\partial y^2} + D\frac{\partial^2 A}{\partial y^2} - C\frac{\partial^2 B}{\partial y^2}\Big)_j\Big]$$

$$(\bar{P}\cdot\bar{K}) = \frac{-1}{\Delta pN}\sum_{j=0}^{N}(F_j\cdot\bar{\omega}_j)$$

$$(\bar{K}\cdot T_2) = \frac{-K_2}{N\,f_o^{\,2}}\sum_{j=0}^{N}\Big[\Big(\frac{\partial^2 F}{\partial y^2}\Big)_j\cdot F_j\Big]$$

$$(K'\cdot T_2)(k) = \frac{K_2}{2Nf_o^{\,2}}\sum_{j=0}^{N}\Big[k^2(C^2 + D^2)_j - \Big(C\frac{\partial^2 C}{\partial y^2} + D\frac{\partial^2 D}{\partial y^2}\Big)_j\Big]$$

$$(\bar{K}\cdot T_4) = \frac{-K_4}{N\,f_o^{\,2}}\sum_{j=0}^{N}(E - F)_j\cdot\Big(\frac{\partial^2 E}{\partial y^2} - \frac{\partial^2 F}{\partial y^2}\Big)_j$$

$$(K'\cdot T_4)(k) = \frac{K_4}{2Nf_o^{\,2}}\sum_{j=0}^{N}\Big\{-A_j\Big[\Big(\frac{\partial^2 A}{\partial y^2} - \frac{\partial^2 C}{\partial y^2}\Big)_j - k^2(A-C)_j\Big]$$

$$- B_j\Big[\Big(\frac{\partial^2 B}{\partial y^2} - \frac{\partial^2 D}{\partial y^2}\Big)_j - k^2(B-D)_j\Big]\Big\}$$

The energy transformations of the m wave disturbance have been omitted for brevity. By replacing k, A, B, C, and D with m, G, H, P, and Q, the entire transformation set will be complete.

VII. INITIAL CONDITIONS

A natural initial state would be one of no motion and constant temperature. Then the system could run until a steady state is reached or some type of instability occurs. However, to save computer time, the initial state was chosen to be near a critical state for development of the most unstable wave.

When the mean flow model was allowed to run with no disturbance, the wind field reached a steady state; the Reynolds stresses balanced the heat input. This steady state was comprised of a meridional Hadley cell superimposed on the zonal flow. This Hadley cell mean flow was utilized as the initial condition.

If we set $\frac{\partial}{\partial t} \equiv 0$ and A-D, G-Q $\equiv 0$,

the F equation yields $0 = K_4 \frac{\partial}{\partial y}(\frac{\partial E}{\partial y} - \frac{\partial F}{\partial y})$,

the E equation yields $0 = -\mu^2 \varkappa h(\frac{W}{2} - y)/W - K_2 \frac{\partial^2 F}{\partial y^2}$.

The solution for F is:

$$F = \frac{\mu^2 \varkappa h}{K_2} \left(\frac{y^2}{4} - \frac{y^3}{6W}\right) \qquad (7.1)$$

This solution requires that E = F which implies that $\phi_M = \phi_T$. In this case

$$\bar{u}_3 = 0 \text{ and } \bar{u}_1 = 2u_T = 2u_M \ .$$

Pedlosky (1964) derived a simple stability criterion for the mean flow. If the potential vorticity gradient $(\frac{\partial q}{\partial y})$ changes sign in either the y-direction or the vertical instability is possible.

For this model $\partial q/\partial y$ is given by

$$\frac{\partial q'}{\partial y} = \beta_o - \frac{\partial^2 \bar{u}_1}{\partial y^2} + \frac{\mu^2}{2}(\bar{u}_1 - \bar{u}_3) \qquad (7.2)$$

$$\frac{\partial q^3}{\partial y} = \beta_o - \frac{\partial^2 \bar{u}_3}{\partial y^2} - \frac{\mu^2}{2}(\bar{u}_1 - \bar{u}_3) \qquad (7.3)$$

Although $\bar{u}_3 = 0$ initially, easterlies and westerlies develop with time as observed in the earth's atmosphere. However, because $\bar{u}_3 \ll \bar{u}_1$, we shall neglect $\bar{u}_3$ for this discussion.

If we neglect $\bar{u}_3$ in equation (7.3), we see that

$$\beta_o = \frac{\mu^2}{2}\bar{u}_1$$

is the critical value of the mean flow. Above that value, instability may occur for some wave number. If we solve for $\bar{u}_{1\ \text{critical}}$ a value of h_{critical} may be derived through the Hadley cell initial condition (7.1). In this paper

$$h_{\text{critical}} = 0.0011$$

The disturbance initial conditions are

$A = 200 \sin \pi y/w$

$B, C, D = 0$

$G = 200 \sin \pi y/w$ after 100 days

$H, P, Q = 0$

VIII. RESULTS

A. HIERARCHY OF UNSTABLE WAVE NUMBERS

The objective of the first experiment was to find a hierarchy of wave numbers in order of wave growth for a particular mean flow. The mean flow was given by the Hadley cell solution with $h = 0.004$ kj ton^{-1} s^{-1} and it was held constant with time. Since the mean flow did not vary with time, the equations for the disturbance became linear. Each case was run until expotential growth was achieved. Figure 3 shows the graphs of wave number vs wave growth rate for two sets of conditions: $\beta_o = 0$ and $\beta_o = 1.67 \times 10^{-11}$, and $W = 4{,}000$ km and $W = 8{,}000$ km. The growth rate shown is

$$\text{growth rate} = \frac{1}{t_2 - t_1} \ln \left[\frac{\text{Amp}(t_2)}{\text{Amp}(t_1)}\right] \times 10^7$$

where Amp(t) = amplitude of the disturbance at time t.

Pedlosky (1964) has computed the growth rate for this wind profile using different values for various parameters.

Figure 3 exhibits how the Beta term stabilizes the longer waves.

B. INTERACTIONS BETWEEN WAVE AND MEAN FLOW

The second set of experiments were devised to test the growth of the most unstable amplifying wave, allowing interactions with the mean flow, as a function of heating. All experiments were conducted using Palmen's exchange coefficient of 225×10^{-4} ton m^{-1} s^{-1} and heat = h_{critical} (0.001 kj ton^{-1} s^{-1}) as the initial condition for the Hadley cell.

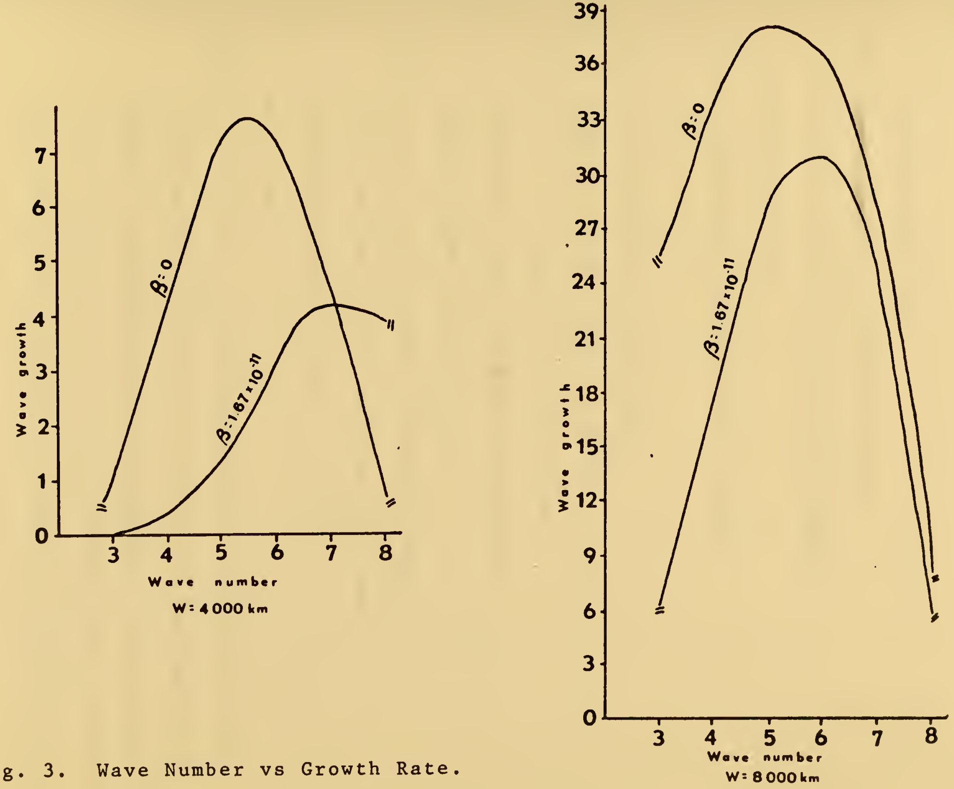

Fig. 3. Wave Number vs Growth Rate.

Each experiment was run for 300 days. The k wave was introduced immediately; the m wave (if existed) was introduced at 100 days.

The following tables were set up to briefly describe the characteristics of each wave number by way of symbolic nomenclature. The symbols are:

D = wave dies immediately

N = a non-steady wave, disturbance energy oscillates up and down as the wave interacts with the mean flow.

SW = a steady wave, total disturbance energy is = ( ) $m^2 s^{-2}$.

Peak - the peak amount of disturbance energy = ( ) $m^2 s^{-2}$ at _____day.

E'(k) vs E'(m) - comparison of k and m wave disturbance energy over the 200 day period when both waves are introduced.

E'(m) > E'(k) - if the m wave disturbance energy did exceed that of the k wave, then the m wave disturbance energy, E'(m) = ( ) $m^2 s^{-2}$ on ____day.

$\overline{S}\cdot\overline{P}$ = ( ) kj $m^{-2} s^{-1}$ is the average amount of conversion of heat to APE usually computed after the mean flow has come to some degree of equilibrium with the disturbance. If the system has not run long enough to reach the equilibrium, then the value is given which best represents the average $\overline{S}\cdot\overline{P}$ thus far incurred.

$\beta = 1.67 \times 10^{-11}$

w = 4,000 km k=7 no m

		k wave			m wave					
heat	exp	growth begins	peak	type	growth begins	peak	type	$E'(k)$ vs $E'(m)$	$E'(m) > E'(k)$?	$\bar{S}\cdot\bar{P}$ ($\times 10^{-4}$)
.0011	1			D						0.3
0.002	2			D						0.9
0.004	3	Slow at 140 days	(17) at 254 days	SW (9.2)						2.9
0.008	4	fast at 40 days	(77) at 80 days	SW (41)						5.8
0.012	5	fast at 30 days	(124) at 56 days	SW (73)						8.8
0.016	6	very fast at 20 days	(166) at 44 days	SW (105)						12

Table 5.1

$\beta = 1.67 \times 10^{-11}$
$w = 8{,}000$ km $k=6$ no m

heat	exp	k wave			m wave					
		growth begins	peak	type	growth begins	peak	type	$E'(k)$ vs $E'(m)$	$E'(m) > E'(k)$?	$\overline{S} \cdot \overline{P}$ ($\times 10^{-4}$)
.0011	7			D						1.4
0.002	8	very slowly at 220 days	(11) at 324 days (run 600	N days)						3.8
0.004	9	very slowly at 60 days	(101) at 136 days	N						7.1
0.008	10	moderately at 28 days	(179) at 76 days	N						16
0.012	11	fast at 20 days	(273) at 58 days	N						25
0.016	12	fast at 20 days	(465) at 56 days	N						38

Table 5.2

$\beta = 1.67 \times 10^{-11}$

$w = 4{,}000$ km $k=7$ $m=6$ at 100 days

		k wave			m wave					
heat	**exp**	**growth begins**	**peak**	**type**	**growth begins**	**peak**	**type**	$E'(k)$ vs $E'(m)$	$E'(m) > E'(k)$?	$\bar{S} \cdot \bar{P}$ ($\times 10^{-4}$)
0.002	13			D						0.9
0.004	14	very slowly at 140 days	(16) at 270 days	SW			D	k>>m		2.9
0.008	15	fast at 40 days	(77) at 80 days	SW (41)			D	k>>m		5.8
0.012	16	fast at 28 days	(122) at 54 days	SW (73)			D	k>>m		8.8
0.016	17	very fast at 20 days	(165) at 45 days	SW (105)			D	k>>m		12

Table 5.3

$\beta = 1.67 \times 10^{-11}$

w = 8,000 km k=6 m=5 at 100 days

		k wave			m wave					
heat	**exp**	**growth begins**	**peak**	**type**	**growth begins**	**peak**	**type**	$E'(k)$ vs $E'(m)$	$E'(m) > E'(k)$?	$\bar{S}\cdot\bar{P}$ ($x10^{-4}$)
0.002	18	dies initially grows very slowly at 200 days	Still growing at 300 days (1.8)				D			3.8
0.004	19	slowly at 60 days	(102) at 142 days	N	very slowly immediately	(17.5) at 188 days	N	k>>m	at 188 days	7.1
0.008	20	fast at 28 days	(179) at 76 days	N	slowly immediately	(50) at 296 days	N	k>m	at 296 days	16
0.012	21	fast at 22 days	(273) at 58 days	N	fast	(58) at 246 days	N	k>m	at 246 days	26.5
0.016	22	fast at 20 days	(465) at 56 days	N	very slowly	(107) at 232 days	N	k>m	at 158 & 212days	36

Table 5.4

$\beta = 1.67 \times 10^{-11}$

w = 4,000 km   k=7   m=8 at 100 days

		k wave			m wave					
heat	exp	growth begins	peak	type	growth begins	peak	type	$E'(k)$ vs $E'(m)$	$E'(m) > E'(k)$?	$\bar{S}\cdot\bar{P}$ ($\times 10^{-4}$)
0.008	23	fast at 40 days (like #15)	(77) at 80 days	SW (41)			D	k>>m		5.8
0.016	24	very fast at 20 days (like #17)	(165) at 45 days	SW (105)			D	k>>m		12

Table 5.5

$\beta = 1.67 \times 10^{-11}$

w = 8,000 km k=6 m=7 at 100 days

		k wave			m wave					
heat	**exp**	**growth begins**	**peak**	**type**	**growth begins**	**peak**	**type**	**$E'(k)$ vs $E'(m)$**	**$E'(m) > E'(k)$?**	**$\bar{\zeta} \cdot \bar{P}$ ($\times 10^{-4}$)**
0.008	25	fast at 28 days (like #20 1st 100 days)	(179) at 76 days	N	slowly immediately	(90) at 280 days	N	m>k	at 166 days and henceforth	16
0.012	26	fast at 22 days (like #21 1st 100 days)	(273) at 58 days	N	moderately immediately	(126) at 250 days	N	m>k	at 132 & 164 days & henceforth	25
0.016	27	fast at 20 days (like #22 1st 100 days)	(465) at 56 days	N	moderately immediately	(187) at 300 days	N	m>k	usually	36

Table 5.6

$\beta = 1.67 \times 10^{-11}$

w = 8,000 km k=6 m=8 at 100 days

heat	exp	k wave			m wave			$E'(k)$ vs $E'(m)$	$E'(m) > E'(k)$?	$\overline{S}\cdot\overline{P}$ $(x10^{-4})$
		growth begins	peak	type	growth begins	peak	type			
0.008	28	fast at 28 days (like#20 1st 100 days)	(179) at 76 days	N	very slowly immediately	(20) at 262 days	N	k>>m		16
0.012	29	fast at 22 days (like#21 1st 100 days)	(273) at 58 days	N	very slowly immediately	(41) at 290 days	N	k>>m		25
0.016	30	fast at 20 days (like#22 1st 100 days)	(465) at 56 days	N	very slowly immediately	(50) at 268 days	N	k>>m		36

Table 5.7

$\beta = 1.67 \times 10^{-11}$

w = 8,000 km k=6 m=3 at 100 days

		k wave			**m wave**					
heat	**exp**	**growth begins**	**peak**	**type**	**growth begins**	**peak**	**type**	$E'(k)$ vs $E'(m)$	$E'(m) > E'(k)$?	$\overline{S}\cdot\overline{P}$ ($\times 10^{-4}$)
0.008	31	fast at 28 days (like#20 1st 100 days)	(179) at 76 days	N			D	k>>>m		16
0.012	32	fast at 22 days (like#21 1st 100 days)	(273) at 58 days	N	fast at 210 days	(12.4) at 232 days	N	k>>m		26
0.016	33	fast at 20 days (like#22 1st 100 days)	(465) at 56 days	N	fast at 196 days	(15.1) at 250 days	N	k>>m		38

Table 5.8

$\beta = 0$

$w = 4{,}000$km $k=5$ no m

		k wave			**m wave**					
heat	**exp**	**growth begins**	**peak**	**type**	**growth begins**	**peak**	**type**	$E'(k)$ vs $E'(m)$	$E'(m) > E'(k)$?	$\overline{\zeta} \cdot \overline{P}$ $(\times 10^{-4})$
.0011	34			D						0.3
0.002	35			D						0.9
0.004	36	slowly at 44 days	(25) at 100 days	SW (8.4)						1.3
0.008	37	fast at 28 days	(65) at 54 days	SW (22)						2.7
0.012	38	fast at 8 days	(100) at 40 days	SW (35)						4.2
0.016	39	very fast at 8 days	(132) at 34 days	SW (48)						5.7

Table 5.9

$\beta = 0$

w=8,000km k=5 no m

		k wave			m wave					
heat	exp	growth begins	peak	type	growth begins	peak	type	$E'(k)$ vs $E'(m)$	$E'(m) > E'(k)$?	$\overline{S}\cdot\overline{P}$ ($\times 10^{-4}$)
.0011	40	fast at 4 days	(28.5) at 44 days	Wave de-clines*						0.6
0.002	41	fast immediately	(37) at 42 days	N						1.2
0.004	42	fast immediately	(58) at 38 days	N						2.8
0.008	43	fast immediately	(115) at 34 days	N						7.2
0.012	44	fast immediately	(175) at 30 days	N						12
0.016	45	fast immediately	(231) at 26 days	N						18

*to (0.2) at 138 days then grows slowly

Table 5.10

C. $\bar{u}_1$ AND $\bar{u}_T$ VERSUS HEATING FOR THE STEADY WAVE EXPERIMENTS

The table below shows the dependence of the zonal flow upon the net heating rate for the Steady Wave experiments.

heat (kj ton^{-1} s^{-1}	exp#	$\bar{u}_T$(m s^{-1})	$\bar{u}_1$(m s^{-1})
0.004	3	6.9	14.1
0.008	4	7.1	15.1
0.012	5	7.2	15.6
0.016	6	7.2	16.0

Table 5.11

Table 5.11 lists the steady state values of the zonal flow. The rather small increases in $\bar{u}_T$ with heat is best explained by the rapid baroclinic response to the wind sheer decaying the unstable zonal flow.

D. A BAROCLINIC, STEADY WAVE

Experiment #5 $\left(\begin{array}{ll} \beta_o & = 1.67 \times 10^{-11} \\ w & = 4{,}000 \text{ km} \\ k & = 7 \\ \text{heat} & = 0.012 \end{array}\right)$, exhibits a

very interesting feature in this model: a steady, baroclinic wave. Figure 4 is a graph of mean kinetic energy, $\bar{K}$, mean potential energy, $\bar{P}$, mean energy, $\bar{E}$, and total energy, E, for experiment #5. Initially, the mean flow grows rapidly, as shown on Figure 4, with negligible disturbance energy. At the 40th day, the zonal mean flow has reached

its peak and decreases rapidly while the disturbance begins to grow. By the 115th day, the entire atmosphere has reached a steady state.

Initially, the maximum $\overline{u}_1 = 4.9$ m s^{-1} and $\overline{u}_T = 2.4$ m s^{-1}. At the 20th day, the maximum $\overline{u}_1 = 14.2$ m s^{-1} (henceforth, whenever zonal mean flow is mentioned, it will mean the maximum speed in the north-south column) and $\overline{u}_T = 7.5$ m s^{-1}. The 40th day exhibited the maximum mean flow energy, due to the maximum $\overline{P}$, with $\overline{u}_1 = 21.7$ m s^{-1} and $\overline{u}_T = 11.1$ m s^{-1}. However, the winds continued to increase until the 46th day, as attested to by the $\overline{K}$ graph, with $\overline{u}_1 = 25.3$ m s^{-1} and $\overline{u}_T = 10.9$ m s^{-1}.

Figure 5 (E'(k)) portrays how the wave grew beginning at the 32nd day. By the 38th day, the wave responds to the strong baroclinic instability, as shown by the large $\overline{u}_T$, and grows expotentially. Barotropic damping $(K'\cdot\overline{K})$ occurs exclusive of any barotropic growth the entire cycle of the wave, and exhibits large oscillations during the rapid growth of the wave.

The wave continued to grow by baroclinic instability until the 56th day when the wave reached its peak energy with a disturbance energy, E', = 123 m^{2} s^{-2}. By this time, the thermal wind had decreased from a peak of 11.2 m s^{-1} on the 42nd day to 7.5 m s^{-1} on the 56th day, destroying the source of the baroclinic growth.

On the 38th day, when the wave began its large baroclinic growth, barotropic damping begins to reach its greatest value as seen in Fig. 5. Initially, as the barotropic damping oscillates about its mean of 1.4x 10^{-5}kj ton^{-1}s^{-1},the baroclinic instability is by far dominant. However, by the 58th day, barotropic damping plus the loss of eddy kinetic energy, K', by frictional dissipation becomes larger than $P'\cdot K'$; hence, baroclinic effects must be diminishing.

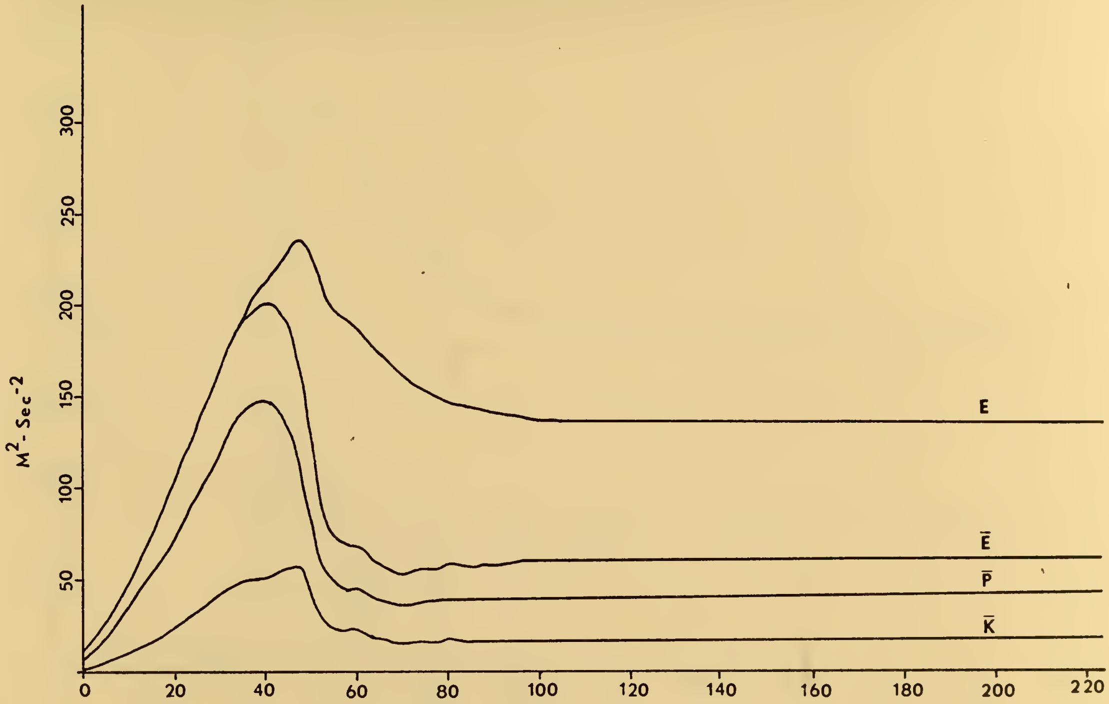

Fig. 4. Energies vs Time in Days for Exp #5.

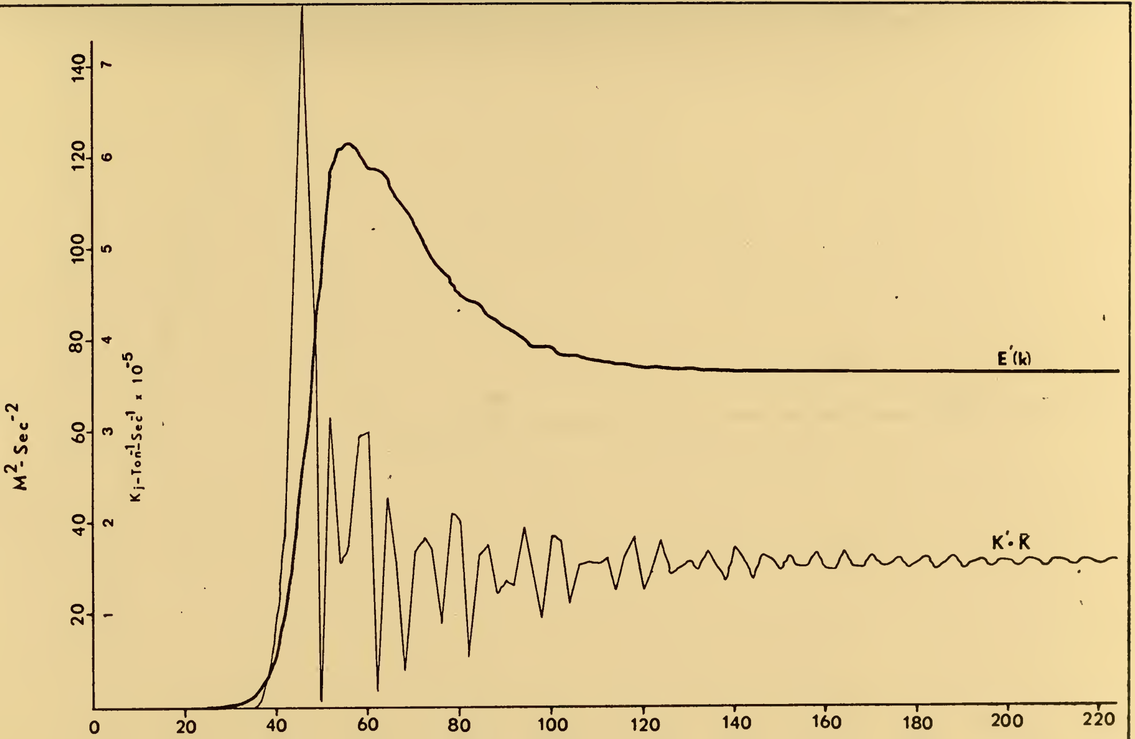

Fig. 5. Disturbance Energy (k) and Barotropic Transformation vs Time for Exp #5.

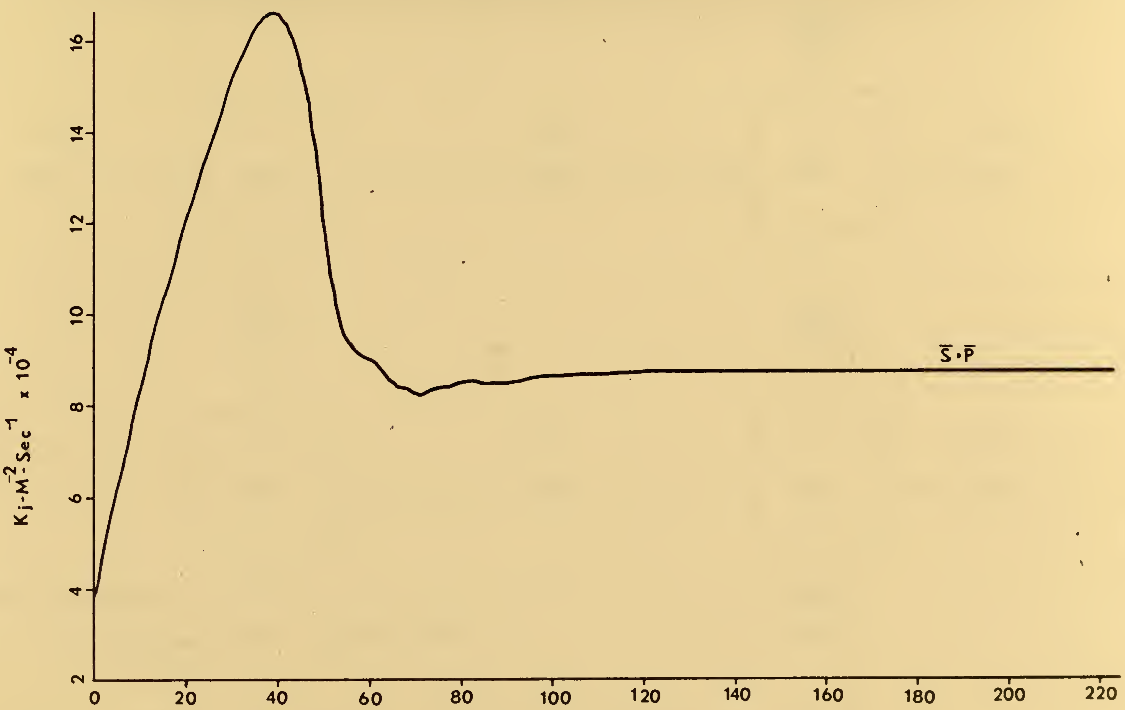

Fig. 6. Conversion of Net Heating to Available Potential Energy for Exp #5.

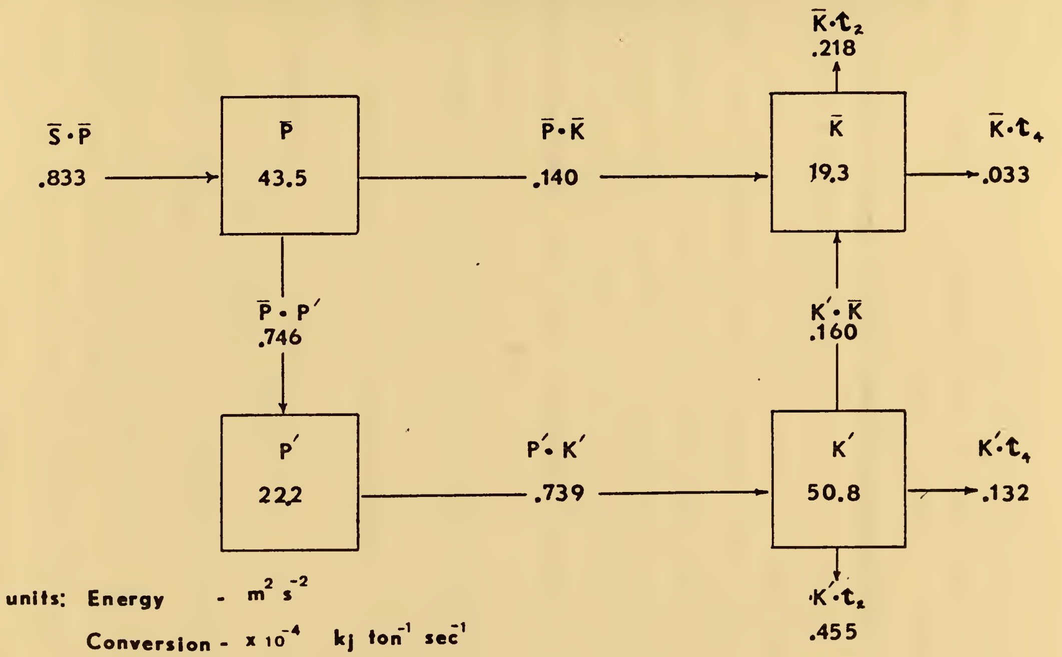

Fig. 7. Energy Flow Diagram at 300 days for Steady Wave Exp #5.

As the barotropic damping reaches steady state, it appears to come into equilibrium with baroclinic growth, hence, the steady state of the disturbance energy.

Figure 6 is a graph of the conversion of net heating to available potential energy ($\overline{S}\cdot\overline{P}$). The graph shows the rapid rise of $\overline{S}\cdot\overline{P}$ to a peak of 16 x 10^{-4}kj m^{-2} s^{-1} in a vertical column (1.6 x 10^{-4}kj ton^{-1} s^{-1}) at 40 days, then its decrease to the steady state value of 8.8 x 10^{-4}kj m^{-2} s^{-1} by the 104th day.

At the end of the 300th day run, the entire atmosphere has been at a steady state equilibrium since the 115th day. The energy conversion terms feeding $\overline{P}$, P', $\overline{K}$, and K' were constant with respect to time, as were the energy terms; therefore, the conversion terms should balance for each energy term. Figure 7 is a pictorial display of the 300th day energy flow after Phillips (1956), the only conversion not balancing being the ($\overline{K}\cdot\tau_4$).

In summary, the steady wave is achieved by the conversion of $\overline{P}$ to K' which is ultimately balanced by frictional losses and barotropic damping through the action of the Reynolds stresses.

E. A NON-STEADY WAVE WITH BAROTROPIC EFFECTS

Experiment #12 $\left(\begin{array}{lcl} \beta_o & = & 1.67 \times 10^{-11} \\ w & = & 8{,}000 \text{ km} \\ k & = & 6 \\ \text{heat} & = & 0.016 \end{array}\right)$, exhibits another quite interesting feature, a wave initially amplified by baroclinicity which then grew by barotropic effects.

Figure 8 is a graph of the mean flow energies and total energy for experiment #12. Notice the large and small oscillations in each energy graph and how the total energy graph is smoother than the mean flow

energy graph. This is due to the disturbance drawing energy from the mean flow and vice versa. So when the disturbance decreases, the mean flow increases and vice versa which tends to smooth out the total energy graph.

On the 20th day, the wave grew rapidly by baroclinic effects. At that time, $\bar{u}_T = 9.3 \text{ m s}^{-1}$ and $\bar{u}_1 = 18.1 \text{ m s}^{-1}$ while on the 30th day, $\bar{u}_T = 10.9 \text{ m s}^{-1}$ and $\bar{u}_1 = 30.0 \text{ m s}^{-1}$. Since only barotropic damping was occurring and the mean flow increased since the initial 10 days of growth, baroclinic effects amplified the wave to its initial peak of $69.4 \text{ m}^2 \text{ s}^{-2}$ at 30 days.

Figure 9 is a graph of the disturbance energy and the barotropic instability. It may be seen that the barotropic growth term feeds or damps the disturbance. At day 30, the wave has peaked due to baroclinic growth. From the 31st to the 33rd day, the baroclinic instability subsided and the barotropic damping destroyed over half of the wave energy and increased the mean flow to $\bar{u}_T = 15.3 \text{ m s}^{-1}$ and $\bar{u}_1 = 38.2 \text{ m s}^{-1}$.

The 34th is the first day that barotropic instability occurred and although it only lasted for two days, the disturbance peaked at $77 \text{ m}^2 \text{ s}^{-2}$. On the 37th day, barotropic damping again diminished the disturbance until the 40th day. On the 37th day, $\bar{u}_T = 14.1 \text{ m s}^{-1}$ and $\bar{u}_1 = 37.9 \text{ m s}^{-1}$ while on the 40th day, $\bar{u}_T = 17.2 \text{ m s}^{-1}$ and $\bar{u}_1 = 42.6 \text{ m s}^{-1}$.

To further supplement this discussion, the $\bar{K}$ graph is given on the bottom of Figure 8, without its energy scale. The graph helps to portray the barotropic damping effect, gain of mean flow energy to the disturbance and vice versa.

On the 40th day, the barotropic instability causes explosive amplification of the wave. However, in the 42nd and 43rd days, barotropic damping occurs and explosive baroclinic growth of approximately five times the average P'•K' takes over.

This baroclinic growth can be seen on the small growth of the $\overline{K}$ graph from the initial loss due to barotropic growth from the 40th to the 42nd day to the small gain from the 42nd to the 44th day.

From the 44th to the 53rd day, growth is a combination of barotropic and baroclinic effects. Possibly the barotropic term is dominant, as with each barotropic damping, the disturbance graph changes slope or declines, hence a greater dependence on barotropic growth. The mean flow has declined greatly due to both a baroclinic and barotropic drain on it, as shown by the 44th day $\overline{u}_T = 14.2$ m s^{-1} and $\overline{u}_1 = 40.5$ m s^{-1} while on the 53rd day, $\overline{u}_T = 11.9$ m s^{-1} and $\overline{u}_1 = 23.9$ m s^{-1}.

From the 53rd to the 82nd day, the wave damped for the most part due to barotropic effects, although a small amount of baroclinic damping does occur.

The disturbance peaks on the 56th day, due to barotropic and baroclinic growth, with the $\overline{K}$ graph reaching its minimum on the 55th day. Again, baroclinic effects do create growth in the wave as seen when barotropic damping is occurring and the disturbance pauses from its decay to grow for a day, then continue its decay.

Figure 10 is included to observe the variation of $\overline{S}\cdot\overline{P}$ term in a non-steady wave. Figure 11 is included to show the many oscillations of the $\overline{P}\cdot\overline{K}$ term (thin line). An interesting phenomenon noted on Figure 11 is the comparison of the $\overline{P}\cdot\overline{K}$ conversion with the $\overline{K}$ term (heavy line, without energy scale). The two terms tend to counteract each other

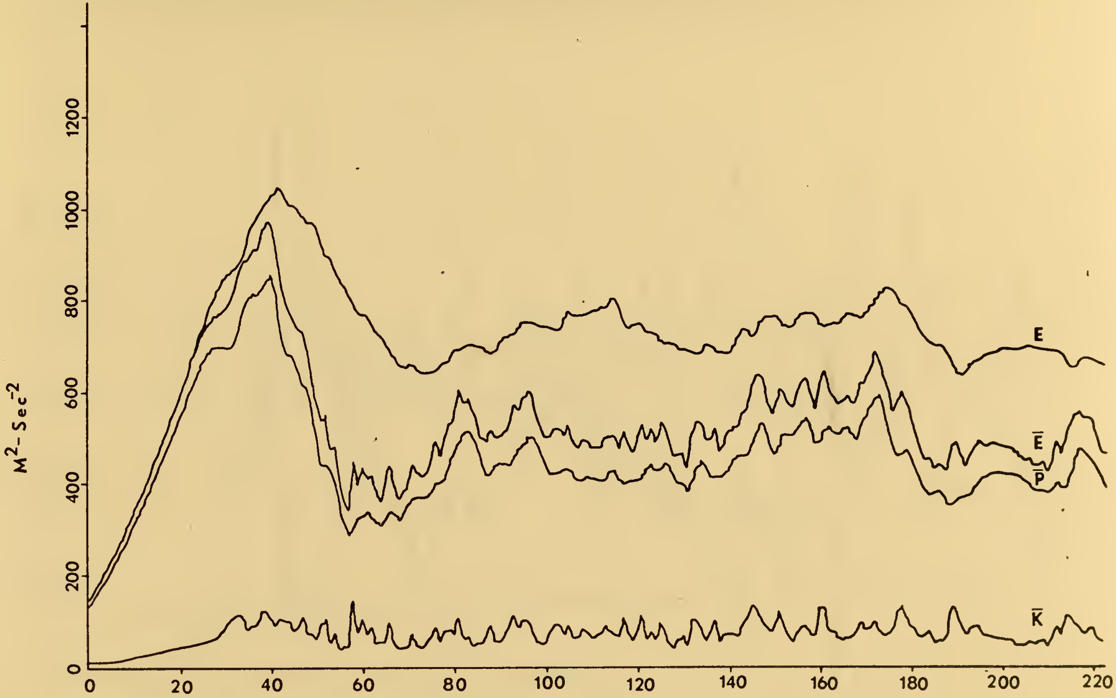

Fig. 8. Energies vs Time in Days for Exp #12.

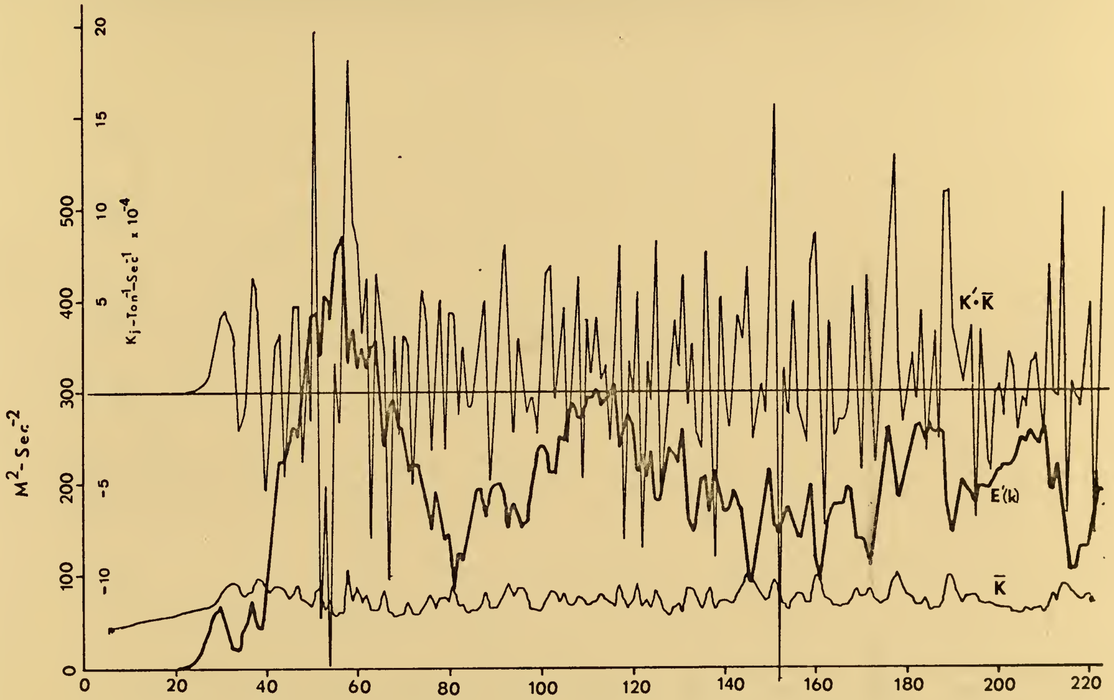

Fig. 9. Disturbance Energy (k), Barotropic Term, and Mean Kinetic Energy vs Time for Exp #12.

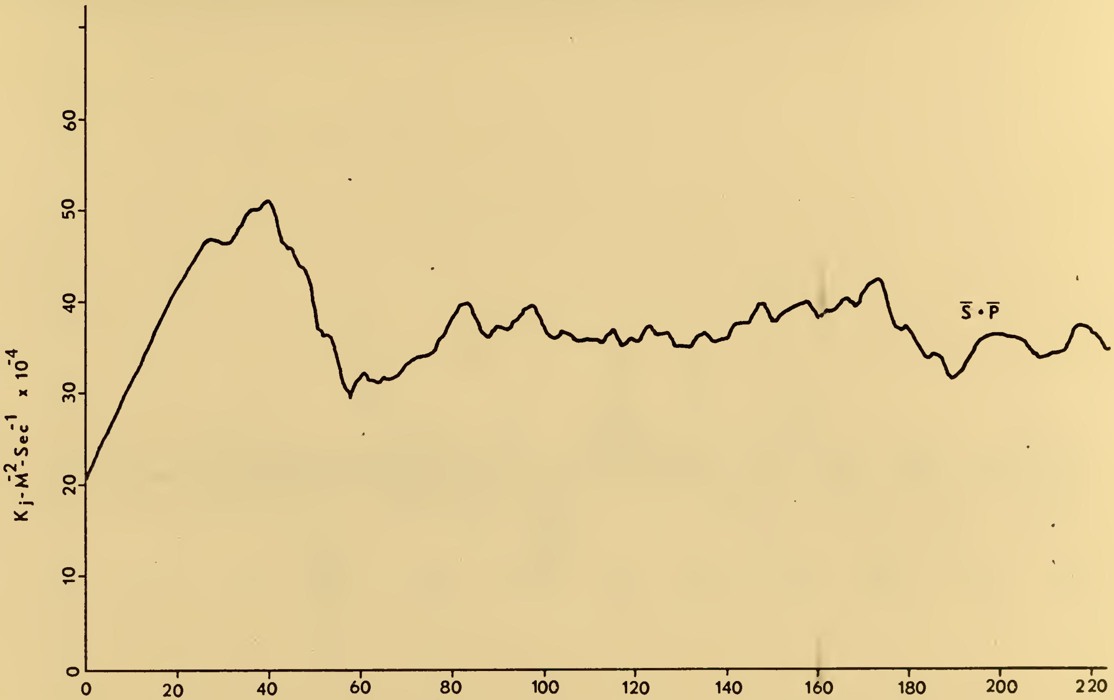

Fig. 10. Conversion of Net Heating to Available Potential Energy for Exp#12

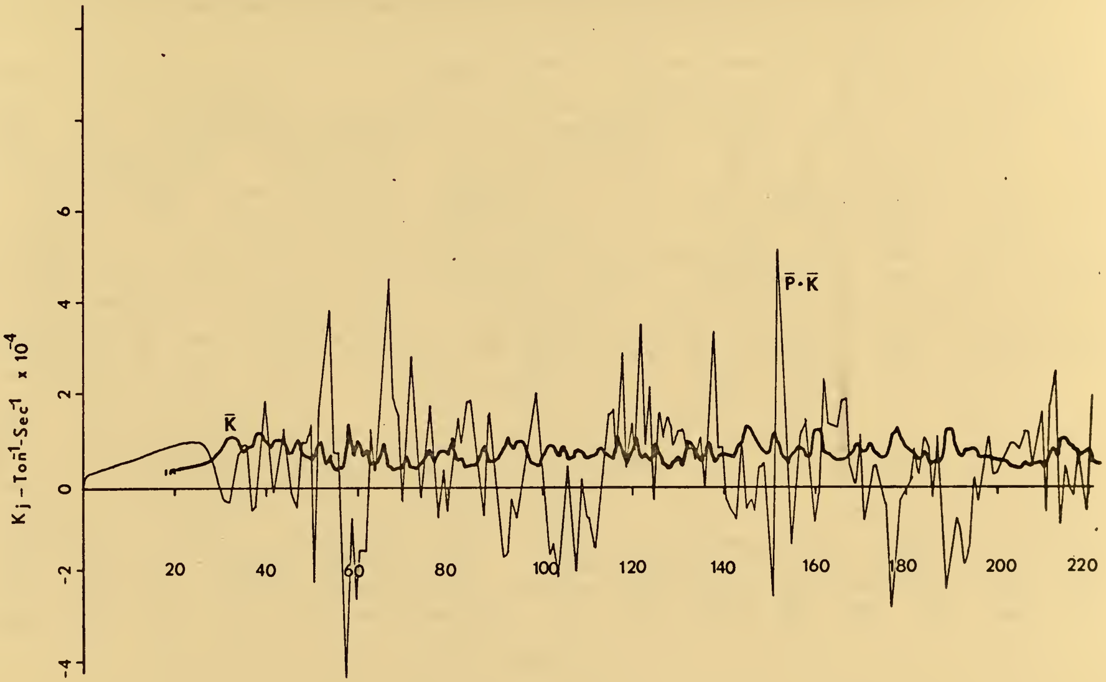

Fig. 11. $\overline{P}\cdot\overline{K}$ and $\overline{K}$ vs Time for Exp #12.

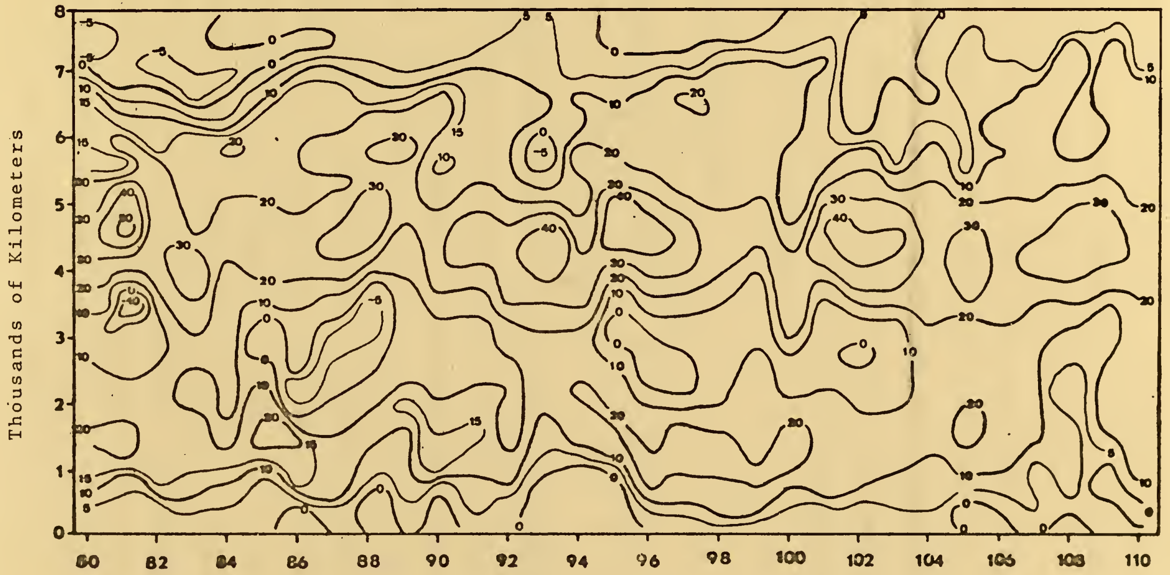

Fig. 12. $\overline{U}_1$ vs Time for Exp #12.

rather than reinforce each other. In the same fashion, $K'\cdot\overline{K}$ also counteracts the $\overline{P}\cdot\overline{K}$ conversion with $K'\cdot\overline{K}$ on the average dominating $\overline{P}\cdot\overline{K}$. Hence with barotropic damping, ($K'\cdot\overline{K} > 0$) the $\overline{P}\cdot\overline{K}$ conversion usually becomes negative. The reverse also occurs.

Figure 12 is a graph of the $\overline{u}_1$ flow with respect to time. The graph begins when the disturbance and mean flow reach a state of equilibrium after the initial growth period of the disturbance on the mean flow. The graph runs from 80 to 110 days. The easterlies present at 250 mb are attributed to the fact that no horizontal diffusion is present in the vorticity equation.

F. A TWO WAVE EXPERIMENT

Experiment #12 $\left(\begin{array}{l} \beta_o = 1.67 \times 10^{-11} \\ w = 8{,}000 \text{ km} \\ k = 6 \\ m = 7 \\ \text{heat} = 0.012 \end{array}\right)$, is one of the few experiments conducted where $E'(m) > E'(k)$. The explanation for the dominance of the m wave over the k wave, in opposition to the results of section V. A., is attributable to the modification of the mean zonal flow by the k wave. Figure 13 is a graph of $E'(k)$ and $E'(m)$ versus time. Figure 14 is a graph of the $K'\cdot\overline{K}$ conversions for each wave. It should be noted that, on the average, both conversions act in the same direction in quite varying degrees.

The Pedlosky criteria (7.2 and 7.3) proved to be a necessary condition for baroclinic and barotropic instability. The baroclinic criteria was met for the initial condition and throughout the forecast. The barotropic criteria was met continuously after the 34th day. At no time did barotropic growth occur when the Pedlosky criteria was not met.

Between the 162nd and 164th day, the E'(m) becomes larger than the E'(k) and remains such throughout the run. At this time, both waves are experiencing barotropic instability. However, the m wave is growing and the k wave is decaying.

The time frame, from 162 to 164 days, is explored further on Figures 15, 16 and 17. Figure 15 and 16 is a graph of $P' \cdot K'$ (bold line) and $K' \cdot \overline{K}$(thin line) for waves k and m respectively. A unique difference is apparent between the two waves. The baroclinic conversion $P' \cdot K'$ never approaches zero with the m wave but does many times with the k wave, and even becomes negative. When the baroclinic term becomes negative, baroclinic damping draws from K'. Usually, the $P' \cdot K'$ conversion was positive, thus the waves were experiencing baroclinic growth. On day 164, both waves are experiencing barotropic growth; however, the k wave is undergoing baroclinic decay and the m wave is experiencing baroclinic growth. The energy flow chart is shown below to help explain the growth of the m wave and decay of the k wave.

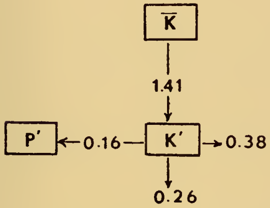

k wave

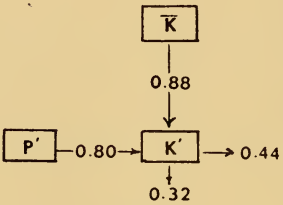

m wave

net change to K'(k)

$= +.61 \text{kj ton}^{-1} \text{ s}^{-1}$

net change to K'(m)

$= +.92 \text{kj ton}^{-1} \text{ s}^{-1}$

Possibly this difference in net inflow to the K' term for each wave gives the growth advantage to the m wave for a ten day period.

If we look at the waves on the 164th day, we find an interesting feature of the barotropic growth. Although the k wave $K' \cdot \overline{K}$ is largest (negative), the m wave is experiencing the growth through baroclinic instability. Since the conversion terms are the meridional average, it is possible the barotropic growth of the m wave in a sector is significantly greater than barotropic growth of the k wave in a similar region. This possibility is explored in Figure 17, a graph of the ϕ'_M phase angle of the k and m waves and $\overline{u}_1$. The wave is experiencing barotropic growth if the tilt of the wave is opposite the shear of the mean flow. Figure 17 depicts the k wave growing barotropically south of the zonal maximum of $\overline{u}_1$ to the easterly jet, and the m wave growing barotropically north of the zonal maximum to about y = 6,000 km, thus demonstrating the greater barotropic instability of the k wave.

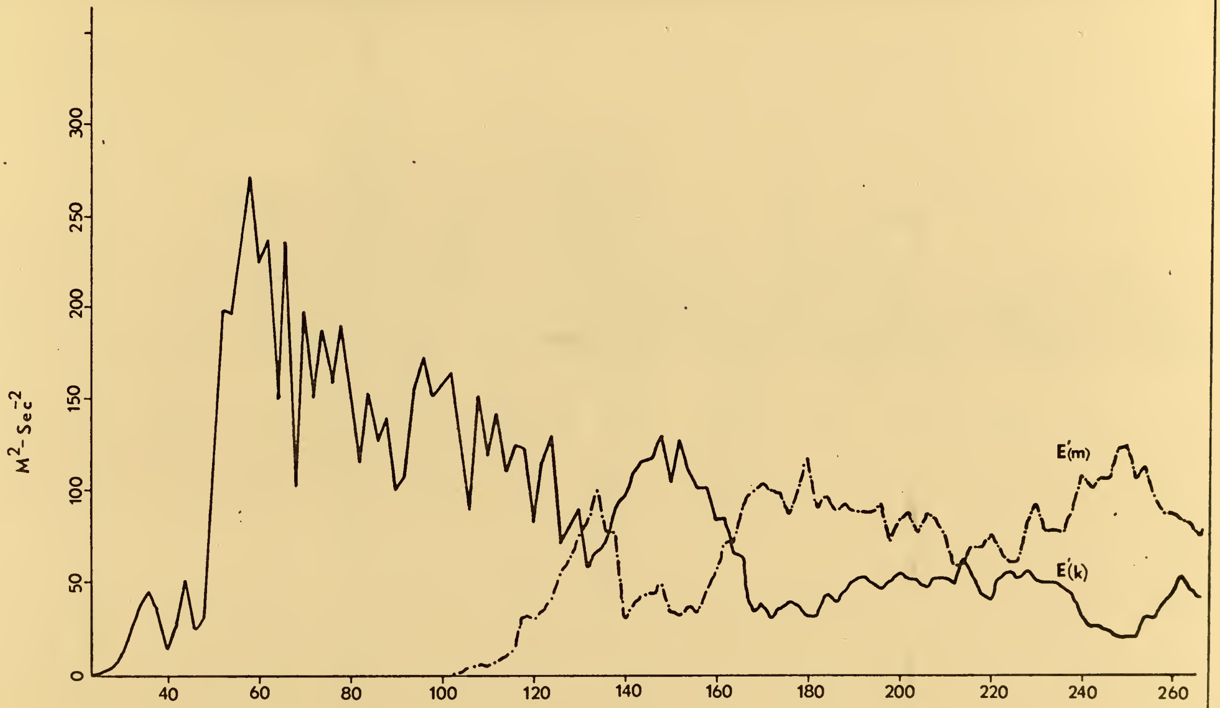

Fig. 13. Disturbance Energies of k wave and m wave for Exp #26.

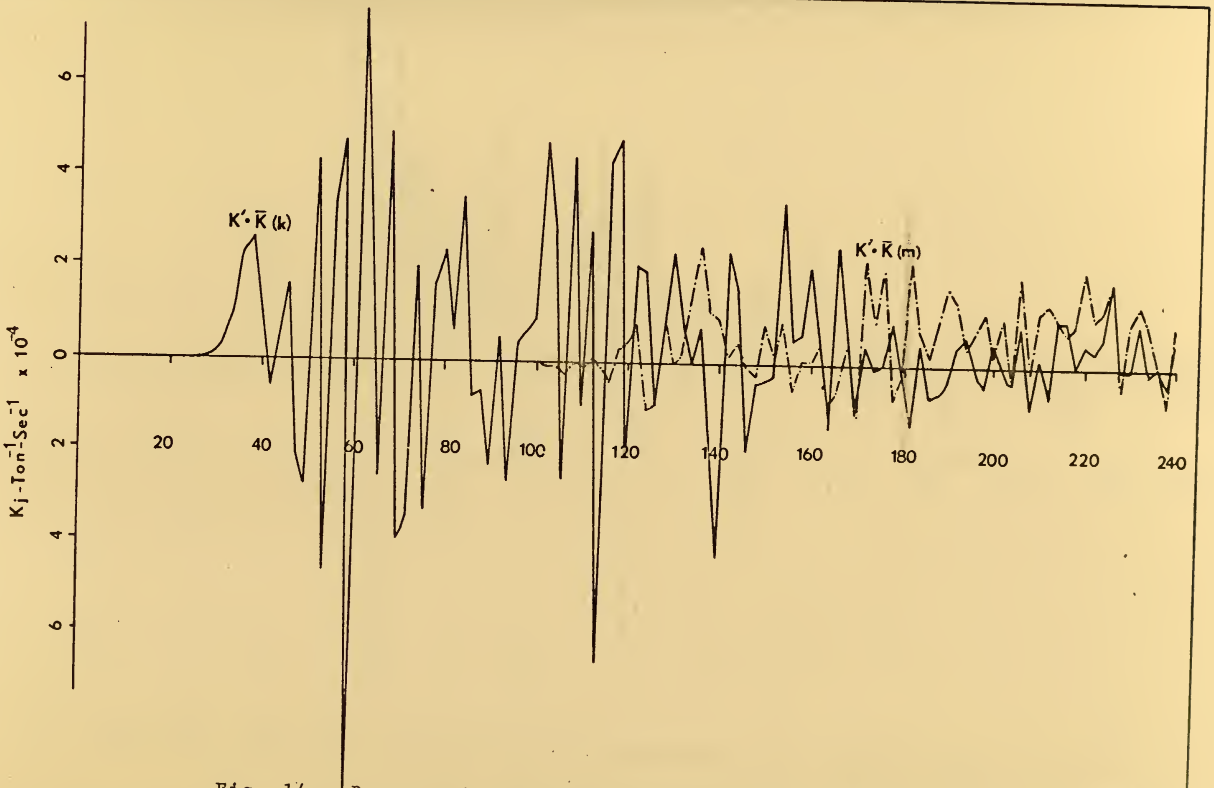

Fig. 14. Barotropic Conversions of k wave & m wave vs Time for Exp#26.

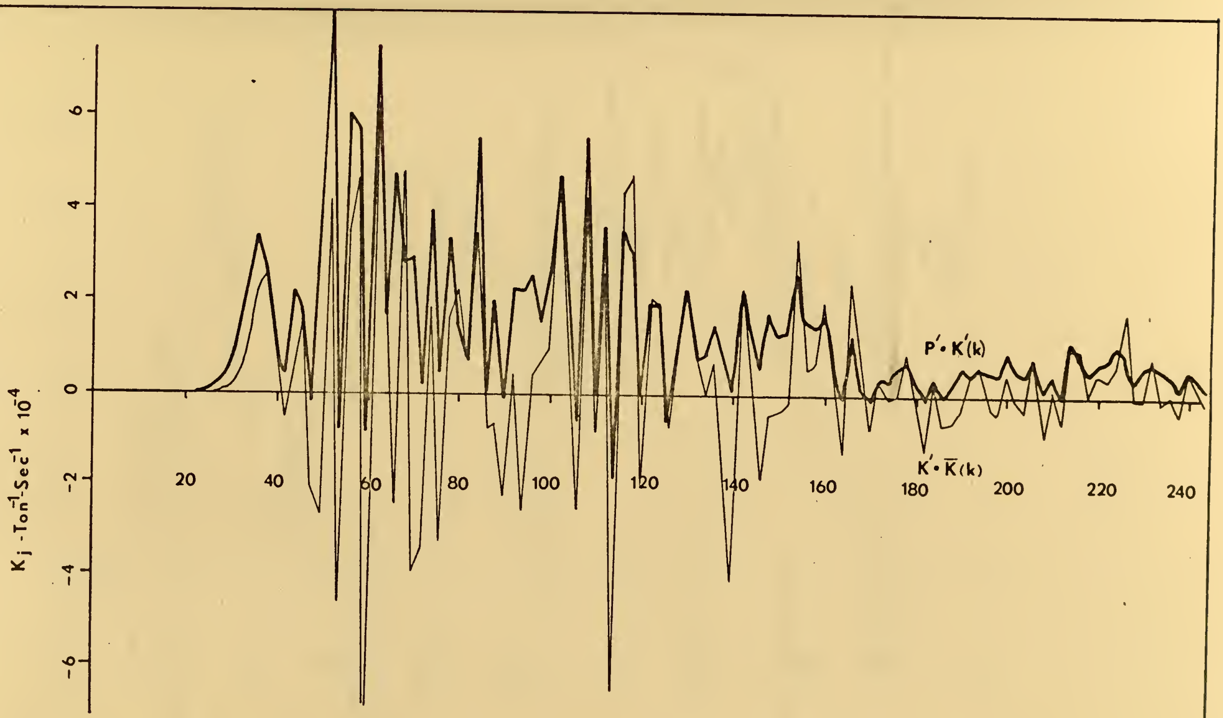

Fig. 15. Baroclinic and Barotropic Conversions of k wave vs Time for Exp #26.

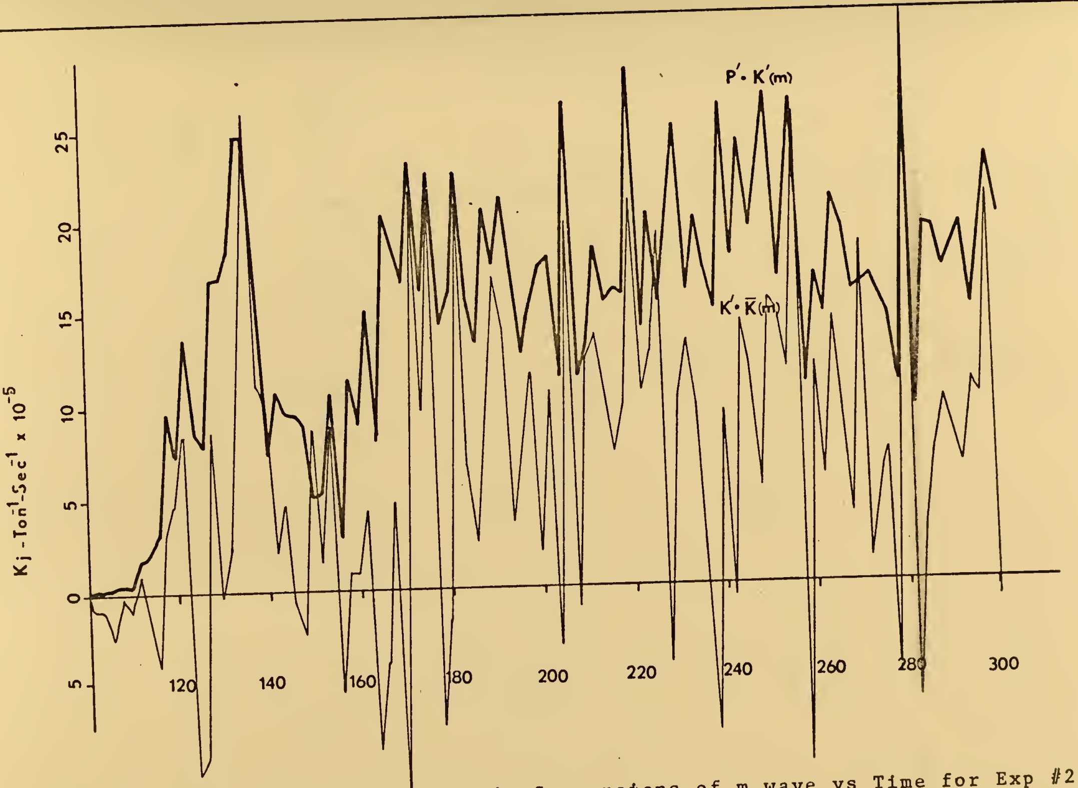

Fig. 16. Baroclinic and Barotropic Conversions of m wave vs Time for Exp #26.

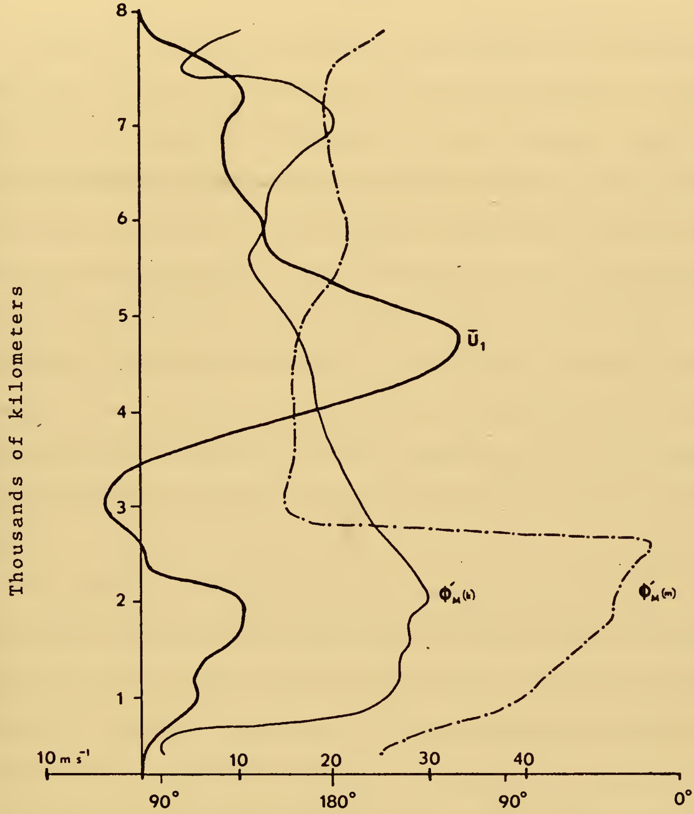

Fig. 17. Phase Angle and $\overline{U}_1$ vs y for Exp #26.

IX. CONCLUSIONS

In order to facilitate physical interpretation of the results, the model was restricted to a mean flow and one or two waves. A steady state solution which was independent of x was obtained. This flow was of the Hadley type with zero mean velocity at level 3 and a parabolic wind profile at level 1. The stability of this mean flow was investigated by performing initial value integrations with the linearized frictionless equations. The calculations were continued until exponential wave growth was achieved. At this point, the growth rates for a range of wave numbers were calculated. The growth rate of the waves was determined as a function of wall separation and β. The growth rate was reduced by the β effect and increased greatly by large wall separations.

The nonlinear frictional equations were integrated from an initial state which consisted of the Hadley mean flow upon which was superimposed the wave number of maximum growth rate. For each combination of heating, β, and wall separation, a 300 day prediction was made with the optimum wave number from the linear study previously mentioned. Each of these forecasts was repeated but at 100 days a new wave was introduced. The purpose here was to determine the largest amplitude wave which would exist on the mean flow, the latter having been modified by nonlinear interactions by the first wave. A total of 45 experiments were made as a function of wall separation, heating, β, and wave number.

Constant amplitude propagating disturbances were obtained in every case where the wall separation was 4,000 km. These experiments

contained cases where $\beta = 0$ and $\beta \neq 0$ as well as a large range in heating rates. The steady waves gained energy through baroclinic conversion processes and lost energy through barotropic decay and friction.

The remaining experiments with the wall separation of 8,000 km produced non-steady waves with fluctuating baroclinic and barotropic interactions. The roles of the different types of instability in the growth and decay of the waves were easily distinguished. When one instability was causing strong growth, the other instability was usually a minimum growth conversion or was decaying the disturbance. The barotropic and baroclinic conversions tended to be out of phase with one another, one a maximum - the other a minimum. The $\overline{P}\cdot\overline{K}$ conversion, however, tended to be a constraint on the $\overline{K}$ term and adjusted to the barotropic term. With strong barotropic damping, the $\overline{P}\cdot\overline{K}$ was negative, while with strong barotropic growth, the $\overline{P}\cdot\overline{K}$ conversion was positive. Hence with strong barotropic decay, the Ferrel cell became dominant over the Hadley cell.

Over the long term mean, the waves obtained a net gain of energy through $P'\cdot K'$ and a net loss of energy through $K'\cdot\overline{K}$. The mean temperature gradient from the south wall to the north wall and the $\overline{S}\cdot\overline{P}$ conversion were directly related to the heating and wall separation. With the largest heating and wall separation, the temperature gradients were somewhat greater than the north-south 500 mb temperature gradients in the earth's atmosphere. This is related to the larger than normal heating used to offset the lack of east-west heating gradient. Even with the largest heating and wall separation, the conversion of heat to available potential energy, $\overline{S}\cdot\overline{P}$, is only about 65% of the average for our atmosphere of 56×10^{-4} kj m^{-2} s^{-1} as estimated by Dutton and

Johnson (1967). This underestimate is also the result of the lack of east-west heating.

The zonal mean flow at level 1 exhibited a definite westerly jet in the mid-latitudes, which sometimes split into a double jet. Due to the lack of a horizontal diffusion term, the horizontal gradients were sometimes quite large and occasionally an easterly jet would appear for a short time. The zonal mean flow at level 3 exhibited the belts of zonal easterlies and westerlies typical of the earth's atmosphere.

In this study, we found with a wall separation of 4,000 km only steady baroclinic waves, and with a wall separation of 8,000 km fluctuating baroclinic and barotropic interactions yield non-steady waves. It was determined that the predominate wave number in the fully developed flow was in every case close to the value determined by the linear stability analysis. In the actual atmosphere, where walls are not present, barotropic instability may be important in giving day to day fluctuations in the mean flow.

LIST OF REFERENCES

1. Dutton, J. A. and D. R. Johnson, 1967: The theory of available potential energy and a variation approach to atmospheric energetics. Advances in Geophysics, Vol. 12, 333-436.

2. Fultz, D. et al, 1959: Studies of thermal convection in a rotating cylinder with some implications for large scale atmospheric motions. Meteorological Monographs, Boston, American Meteorological Society, 4, 21, 104 pp.

3. Herring, J. R., 1963: Investigation of problems in thermal convection. Journal of the Atmospheric Sciences, Vol. 20, 325-338.

4. ______________, 1964: Investigation of problems in thermal convection: Rigid boundaries. Journal of the Atmospheric Sciences, Vol. 21, 277-290.

5. Hide, R., 1953: Some experiments on thermal convection in a rotating liquid. Quarterly Journal of the Royal Meteorological Society, 79, 161.

6. Kasahara, A. and W. M. Washington, 1967: NCAR global general circulation model of the atmosphere. Monthly Weather Review, Vol. 95, No. 7, 389-402.

7. ______________, 1971: General circulation experiments with a six-layer NCAR model, including orography, cloudiness, and surface temperature calculations. Journal of the Atmospheric Sciences, Vol. 28, No. 5, 657-701.

8. Manabe, Syukuro, 1969: The atmospheric circulation and the hydrology of the earth's surface. Monthly Weather Review, Vol. 97, No. 11, 739-774.

9. Manabe, Syukuro and J. Smagorinsky, 1967: Simulated climatology of a general circulation model with a hydrologic cycle: II. Analysis of the tropical atmosphere. Monthly Weather Review, Vol. 95, No. 4, 155-169.

10. Matsuno, J., 1966: Numerical integrations of the primitive equations by a simulated backward difference method. Journal of Meteorological Society of Japan, 44, 76-84.

11. Mintz, Y., 1965: Very long-term global integration of the primitive equations of atmospheric motion. WMO Technical Note No. 66, "WMO-IUGG Symposium on Research and Development Aspects of Long Range Forecasting, Boulder, Colo., 1964," Geneva, 1965, 141-167.

12. Palmén, E., 1955: On the mean meridional circulation in low latitudes of the northern hemisphere in winter and the associated meridional and vertical flux of angular momentum. Societas Scientiarum Fennica, Commentations Physica Mathematicae, Vol. 17, No. 8, 1-33.

13. Pedlosky, J., 1964: The stability of currents in the atmosphere and the ocean. Journal of Atmospheric Science, Vol. 21, 201-219, 342-353.

14. Phillips, N. A., 1956: The general circulation of the atmosphere. A numerical experiment. Quarterly Journal of the Royal Meteorological Society, Vol. 82, No. 352, 123-164.

15. Richtmyer, R. D., 1957: Difference Methods for Initial Value Problems. Interscience Publishers, Inc., New York.

16. Riehl, H., et al, 1951: The North-East trade of the Pacific Ocean. Quarterly Journal of the Royal Meteorological Society, Vol. 77, No. 334, 598-626.

17. Rossby, C. G., and R. B. Montgomery, 1935: The layer of frictional influence in wind and ocean currents. Papers in Physical Oceanography and Meteorology, Vol. 3, No. 3, 101.

18. Smagorinsky, J., 1963: General circulation experiments with the primitive equation, I. The basic experiment. Monthly Weather Review, Vol. 91, No. 3, 99-165.

19. Smagorinsky, J., S. Manabe and J. L. Holloway, Jr., 1965: Numerical results from a nine-level general circulation model of the atmosphere. Monthly Weather Review, Vol. 93, No. 12, 727-768.

INITIAL DISTRIBUTION LIST

		No. Copies
1.	Defense Documentation Center Cameron Station Alexandria, Virginia 22314	2
2.	Library, Code 0212 Naval Postgraduate School Monterey, California 93940	2
3.	Associate Professor Roger T. Williams, Code 51 Department of Meteorology Naval Postgraduate School Monterey, California 93940	10
4.	Lieutenant Glenn Curtis Trumbower, USN Fleet Numerical Weather Central, Naval Postgraduate School Monterey, California 93940	5
5.	Naval Weather Service Command Washington Navy Yard Washington, D. C. 20390	1
6.	Officer in Charge Naval Weather Research Facility Naval Air Station, Building R-48 Norfolk, Virginia 23511	1
7.	Commanding Officer U. S. Fleet Weather Central COMNAVMARIANAS, Box 12 FPO San Francisco, California 96630	1
8.	Commanding Officer Fleet Weather Central Box 31 FPO New York, New York 09540	1
9.	Commanding Officer Fleet Numerical Weather Central Naval Postgraduate School Monterey, California 93940	1
10.	ARCRL - Research Library L. G. Hanscom Field Attn: Nancy Davis/Stop 29 Bedford, Massachusetts 01730	1

11. Director, Naval Research Laboratory 1
Attn: Tech. Services Info. Officer
Washington, D. C. 20390

12. American Meteorological Society 1
45 Beacon Street
Boston, Massachusetts 02128

13. Department of Meteorology 3
Code 51
Naval Postgraduate School
Monterey, California 93940

14. Department of Oceanography 1
Code 58
Naval Postgraduate School
Monterey, California 93940

15. Office of Naval Research 1
Department of the Navy
Washington, D. C. 20360

16. Commander, Air Weather Service 2
Military Airlift Command
U. S. Air Force
Scott Air Force Base, Illinois 62226

17. Atmospheric Sciences Library 1
National Oceanographic Atmospheric Administration
Silver Spring, Maryland 20910

18. Professor Victor Starr 1
Department of Meteorology
M. I. T.
Cambridge, Massachusetts 03139

19. Dr. J. Pedlosky 1
Department of Geophysical Sciences
University of Chicago
Chicago, Illinois 60637

20. Dr. Joanne Simpson 1
Experimental Meteorology Branch
National Oceanographic Atmospheric Administration
Coral Gables, Florida 33124

21. Dr. V. Jurcec 1
United Nations Development Program
Box 982
Cairo, United Arab Republic

22. Dr. A. Huss 1
Department of Meteorology
Hebrew University
Jerusalem, Israel

23. National Center for Atmospheric Research 1
Box 1470
Boulder, Colorado 80302

24. Dr. T. N. Krishnamurti 1
Department of Meteorology
Florida State University
Tallahassee, Florida 32306

25. Dr. Fred Shuman 1
Director
National Meteorological Center
Environmental Science Services Administration
Suitland, Maryland 20390

26. Dr. J. Smagorinsky 1
Director
Geophysical Fluid Dynamics Laboratory
Princeton University
Princeton, New Jersey 08540

27. Professor N. A. Phillips 1
54-1422
M. I. T.
Cambridge, Massachusetts 02139

28. Dr. E. N. Lorenz 1
Department of Meteorology
M. I. T.
Cambridge, Massachusetts 02139

29. Professor J. G. Charney 1
54-1424
M. I. T.
Cambridge, Massachusetts 02139

30. Professor K. Ooyama 1
Department of Meteorology
New York University
University Heights
New York, New York 10453

31. Dr. M. G. Wurtele 1
Department of Meteorology
UCLA
Los Angeles, California 90024

32. Dr. A. Arakawa 1
Department of Meteorology
UCLA
Los Angeles, California 90024

33. Dr. David Houghton 1
Department of Meteorology
University of Wisconsin
Madison, Wisconsin 53706

34. Dr. S. K. Kao 1
Department of Meteorology
University of Utah
Salt Lake City, Utah 84112

35. Dr. J. Holton 1
Department of Atmospheric Sciences
University of Washington
Seattle, Washington 98105

36. Dr. P. Gilman 1
National Center for Atmospheric Research
Box 1470
Boulder, Colorado 80302

37. Dr. P. Thompson 1
National Center for Atmospheric Research
Box 1470
Boulder, Colorado 80302

38. Dr. Peter Stone 1
Pierce Hall
Harvard University
Cambridge, Massachusetts 02138

39. Dr. John Young 1
Department of Meteorology
University of Wisconson
Madison, Wisconsin 53706

40. Dr. George J. Haltiner 1
Chairman, Department of Meteorology
Naval Postgraduate School
Monterey, California 93940

41. Dr. Jerry D. Mahlman 1
Geophysical Fluid Dynamics Laboratory
Princeton University
Princeton, New Jersey 08540

42. Dr. Russell Elsberry 1
Department of Meteorology
Naval Postgraduate School
Monterey, California 93940

43. Commanding Officer 1
Pacific Missile Range
Attn: Geophysics Division
Point Mugu, California 93041

44. Dr. Neil Frank 1
National Hurricane Center
National Oceanographic Atmospheric Administration
Coral Gables, Florida 33124

45. Lieutenant Commander Frank H. Taylor 1
U. S. Fleet Weather Central
Box 113
FPO San Francisco, California 96610

46. Mr. Donald H. Lucas 1
Fernbank Science Center
156 Heaton Park Dr. N.E.
Atlanta, Georgia 30307

47. Lieutenant Commander W. Roger Lambertson 1
Department of Meteorology
Naval Postgraduate School
Monterey, California 93940

48. Dr. Peter J. Gierasch 1
Geophysical Fluid Dynamics Institute
Florida State University
Tallahassee, Florida 32306

49. Dr. Andrew P. Ingersoll 1
Division of Geological and Planetary Sciences
California Institute of Technology
Pasadena, California 91109

50. Dr. Robert L. Haney 1
Department of Meteorology
Naval Postgraduate School
Monterey, California 93940

51. Dr. Ron L. Alberty 1
Department of Meteorology
Naval Postgraduate School
Monterey, California 93940

52. Dr. W. L. Gates 1
Department of Meteorology
Naval Postgraduate School
Monterey, California 93940

53. Dr. Richard Alexander 1
The Rand Corporation
1700 Main Street
Santa Monica, California 90406

54. Commanding Officer 1
Fleet Weather Central
Box 110
FPO San Francisco, California 96610

DOCUMENT CONTROL DATA - R & D

(Security classification of title, body of abstract and indexing annotation must be entered when the overall report is classified)

1. ORIGINATING ACTIVITY *(Corporate author)* Naval Postgraduate School Monterey, California 93940	2a. REPORT SECURITY CLASSIFICATION Unclassified 2b. GROUP

3. REPORT TITLE

General Circulation Experiments with a Two-Level Quasi-Geostrophic Model Including Nonlinear Interaction between Two Waves and the Mean Flow

4. DESCRIPTIVE NOTES *(Type of report and inclusive dates)*

Master's Thesis; March 1972

5. AUTHOR(S) *(First name, middle initial, last name)*

Glenn Curtis Trumbower

6. REPORT DATE March 1972	7a. TOTAL NO. OF PAGES 73	7b. NO. OF REFS 19

8a. CONTRACT OR GRANT NO.	9a. ORIGINATOR'S REPORT NUMBER(S)
b. PROJECT NO.	
c.	9b. OTHER REPORT NO(S) *(Any other numbers that may be assigned this report)*
d.	

10. DISTRIBUTION STATEMENT

Approved for public release; distribution unlimited.

11. SUPPLEMENTARY NOTES	12. SPONSORING MILITARY ACTIVITY Naval Postgraduate School Monterey, California 93940

13. ABSTRACT

Long term numerical integrations were performed with a two-level model utilizing the quasi-geostrophic equation set. Friction was incorporated through the vertical derivative of the eddy stress and heating was applied as a linear function of latitude. The long-term interactions between one or two waves in the zonal direction and the mean flow were examined.

The stability of the initial mean flow was investigated with linearized equations and the most unstable wave numbers were determined. The nonlinear equations were integrated using the most unstable wave in the initial conditions. 300 day forecasts were made with various values of the heating, β, wall separation, and wave number. A second wave number was introduced into the experiments in order to determine the most likely wave number for the fully evolved mean flow. Constant amplitude, baroclinic, propagating disturbances were obtained in every case where the wall separation was 4,000 km. The experiments with the wall separation of 8,000 km produced non-steady waves with fluctuating baroclinic and barotropic interactions.

Security Classification

KEY WORDS	LINK A		LINK B		LINK C	
	ROLE	WT	ROLE	WT	ROLE	WT
baroclinic						
barotropic						
constant amplitude						
eddy stress						
energy transformations						
general circulation						
quasi-geostrophic						
two-level model						
vorticity						

Thesis
T8223 Trumbower
c.1

134943

General circulation experiments with a two-level Quasi-Geostrophic model including non-linear interaction between two waves and the mean flow.

Thesis
T3223 Trumbower
c.1

134943

General circulation experiments with a two level Quasi-Geostrophic model including non-linear interaction between two waves and the mean flow.

thesT8223
General circulation experiments with a t
3 2768 001 88847 2
DUDLEY KNOX LIBRARY